Models of the Reduced Forms of Polyiron-Oxo Proteins: An Asymmetric, Triply Carboxylate Bridged Diiron(II) Complex and Its Reaction with Dioxygen

William B. Tolman, Shuncheng Liu, James G. Bentsen, and Stephen J. Lippard*

Contribution from the Department of Chemistry, Massachusetts Institute of Technology, Cambridge, Massachusetts 02139. *Received July 26, 1990*

Abstract: A diiron(II) model compound having features relevant to the active sites of the reduced forms of the polyiron-oxo proteins hemerythrin (Hr), ribonucleotide reductase (RR), and methane monooxygenase (MMO) has been prepared and characterized by elemental analysis, X-ray crystallography, magnetic susceptibility measurements, and Mössbauer, UV-vis, IR, ^{1}H NMR, and EPR spectroscopy. The X-ray crystal structure of the complex, $[Fe_2(O_2CH)_4(BIPhMe)_2]$ (**1**) (BIPhMe = 2,2′-bis(1-methylimidazolyl)phenylmethoxymethane), reveals that the ferrous ions are bridged by one monodentate and two bidentate (syn-syn) bridging formates, a novel arrangement among diiron compounds. Moreover, the molecule has both five- and six-coordinate iron atoms, an asymmetry that belies its simple formula. Thus, one iron atom is octahedral, with two imidazoles from a BIPhMe ligand and a terminal formate completing its coordination sphere, and the other contains only a BIPhMe in addition to the bridging ligands. The latter metal ion has a distorted trigonal-bipyramidal geometry owing to the presence of a weak interaction (Fe···O = 2.787 (3) Å) with the "dangling" oxygen of the monodentate bridging formate. The inequivalence of the iron atoms in **1** is further manifest by the presence of two overlapping quadrupole doublets in its Mössbauer spectrum (δ_1 = 1.26 mm/s; δ_2 = 1.25 mm/s; ΔE_{Q1} = 2.56 mm/s; ΔE_{Q2} = 3.30 mm/s). Solid-state magnetic susceptibility measurements acquired between 6 and 300 K indicate the absence of significant magnetic exchange interaction in **1**. Consistent with its asymmetric structure and lack of magnetic coupling, large dipolar contributions to the isotropic shifts of **1** are observed in its ^{1}H NMR spectrum. Analysis of the latter was aided by using the diamagnetic shift calibrant $[Zn(BIPhMe)Cl_2]$, which was further characterized by elemental analysis, X-ray crystallography, and IR spectroscopy. An unusually shaped integer spin signal at $g \sim 16$ appears in the EPR spectrum of **1**. In a reaction relevant to the functional activity of RR and MMO and reminiscent of oxidative processes previously characterized in heme-iron chemistry, exposure of **1** to O_2 afforded $[Fe_2O(O_2CH)_4(BIPhMe)_2]\cdot H_2O$ (**2**·H_2O), which was characterized by elemental analysis, X-ray crystallography, magnetic susceptibility measurements, and by Mössbauer, UV-vis, IR, ^{1}H NMR, and resonance Raman spectroscopy. The physical properties of **2** are consistent with the presence of its (μ-oxo)bis(μ-carboxylato)diiron(III) core and are similar to those reported for Hr and other complexes with such bridging units. Proof that the source of the oxo bridge in **2** is dioxygen and not adventitious water was obtained by resonance Raman spectroscopic monitoring of its symmetric Fe-O-Fe vibration (ν_s) after treatment of **1** with $^{18}O_2$[ν_s (Fe-^{16}O-Fe) = 520 cm^{-1}; ν_s (Fe-^{18}O-Fe) = 502 cm^{-1}]. Both oxygen atoms of O_2 are incorporated into product, as indicated by manometric measurements of O_2 uptake revealing consumption of 0.6 (1) equiv per mol of **1**. EPR spectra of solutions of **1** briefly exposed to O_2 and then quickly frozen exhibit a signal with features at g = 1.84 and 1.94 arising from a mixed valent Fe(II)Fe(III) species, a possible intermediate in the conversion of **1** to **2**. Acquisition of EPR power saturation data allowed estimation of an antiferromagnetic exchange coupling constant (J) for this species of −31 (2) cm^{-1}, a value similar to those determined for the mixed valent form of MMO. A mechanism for the oxidation of **1** consistent with these observations and reminiscent of reaction schemes proposed for porphyrin-Fe(II) oxidations is suggested.

The polyiron-oxo proteins, a growing class of biomolecules that feature oxygen-bridged di- or polyiron units at their active sites, have been the subjects of considerable research activity in recent years.[1] Motivation for their study derives largely from the varied, biologically significant, and chemically interesting dioxygen activation reactions that they undergo. Reversible dioxygen binding by hemerythrin (Hr), tyrosyl radical generation that enables production of deoxyribonucleotides by ribonucleotide reductase (RR), and catalytic alkane hydroxylation by methane monooxygenase (MMO) exemplify key processes involving dioxygen that are promoted by diiron centers within these proteins.

The synthetic modeling approach has played an important role in developing our understanding of the structures, magnetic properties, and spectroscopic features of the diiron cores in these proteins. Much of this work has focused on the more readily accessible oxidized forms of the cores. A plethora of (μ-oxo)-diiron(III) complexes[2] containing additional bidentate bridges, specifically carboxylate,[3-5] carbonate,[6] or phosphate[7] groups and

Scheme I

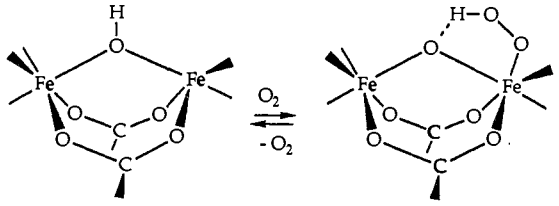

bi-,[3] tri-,[4,6,7] or tetradentate[5] capping ligands has been studied by a variety of physical techniques. As a consequence, accurate

(1) Reviews: (a) Lippard, S. J. *Angew. Chem., Int. Ed. Engl.* **1988**, *27*, 344-361. (b) Lippard, S. J. *Chem. Br.* **1986**, 222-229. (c) Sanders-Loehr, J. In *Iron Carriers and Iron Proteins*; Loehr, T. M., Ed.; VCH Publishers: New York, 1989; pp 373-466. (d) Que, L., Jr.; Scarrow, R. C. In *Metal Clusters in Proteins*; Que, L., Jr., Ed.; ACS Symposium Series No. 372; American Chemical Society: Washington, DC; 1988; pp 152-178.

(2) A recent review: Kurtz, D. M., Jr. *Chem. Rev.* **1990**, *90*, 585-606.

(3) (a) Vincent, J. B.; Huffman, H. C.; Christou, G.; Li, Q.; Nanny, M. A.; Hendrickson, D. N.; Fong, R. H.; Fish, R. H. *J. Am. Chem. Soc.* **1988**, *110*, 6898-6900. (b) Beer, R. H.; Tolman, W. B.; Bott, S. G.; Lippard, S. J. *Inorg. Chem.* **1989**, *28*, 4557-4559.

(4) (a) Armstrong, W. H.; Spool, A.; Papaefthymiou, G. C.; Frankel, R. B.; Lippard, S. J. *J. Am. Chem. Soc.* **1984**, *106*, 3653-3667. (b) Wieghardt, K.; Pohl, K.; Gebert, K. *Angew. Chem., Int. Ed. Engl.* **1983**, *22*, 727. (c) Hartman, J. R.; Rardin, R. L.; Chaudhuri, P.; Pohl, K.; Wieghardt, K.; Nuber, B.; Weiss, J.; Papaefthymiou, G. C.; Frankel, R. B.; Lippard, S. J. *J. Am. Chem. Soc.* **1987**, *109*, 7387-7396. (d) Toftlund, H.; Murray, K. S.; Zwack, P. R.; Taylor, L. F.; Anderson, O. P. *J. Chem. Soc., Chem. Commun.* **1986**, 191-193. (e) Gomez-Romero, P.; Casan-Pastor, N.; Ben-Hussein, A.; Jameson, G. B. *J. Am. Chem. Soc.* **1988**, *110*, 1988-1990. (f) Nishida, Y.; Nasu, M.; Tokii, T. *Inorg. Chim Acta* **1990**, *169*, 143-145. (g) Feng, X.; Bott, S. G.; Lippard, S. J. *J. Am. Chem. Soc.* **1989**, *111*, 8046-8047. (h) Wu, F.-J.; Kurtz, D. M., Jr. *J. Am. Chem. Soc.* **1989**, *111*, 6563-6572. (i) Sessler, J. L.; Sibert, J. W.; Lynch, V. *Inorg. Chem.* **1990**, *29*, 4143-4146.

(5) (a) Yan, S.; Que, L., Jr.; Taylor, L. F.; Anderson, O. P. *J. Am. Chem. Soc.* **1988**, *110*, 5222-5224. (b) Yan, S.; Cox, D. D.; Pearce, L. L.; Juarez-Garcia, C.; Que, L., Jr.; Zhang, J. H.; O'Connor, C. J. *Inorg. Chem.* **1989**, *28*, 2507-2509. (c) Norman, R. E.; Yan, S.; Que, L., Jr.; Backes, G.; Ling, J.; Sanders-Loehr, J.; Zhang, J. H.; O'Connor, C. J. *J. Am. Chem. Soc.* **1990**, *112*, 1554-1562.

0002-7863/91/1513-152$02.50/0

Scheme II

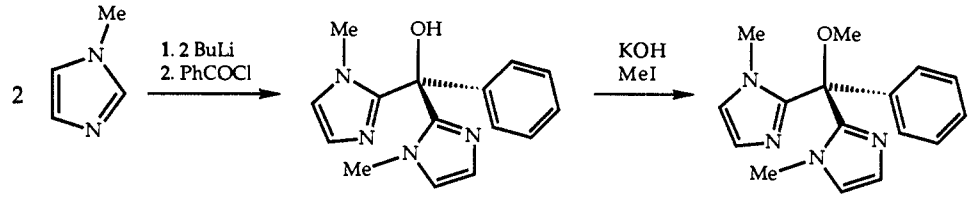

BIPhOH BIPhMe

structural and spectroscopic mimicry of the oxidized protein active sites has been achieved.

Nevertheless, it is the interaction of dioxygen with the reduced diiron(II) centers that is central to the biological functions of Hr, RR, and MMO. In deoxyHr, for example, five imidazoles from histidine residues are bound in an asymmetric array to a (μ-hydroxo)bis(μ-carboxylato)diiron(II) core, leaving a single coordination site available for dioxygen ligation (Scheme I).[8-12] The currently accepted view is that dioxygen binding with concomitant electron transfer(s) from the metal ions, coupled with proton migration from the hydroxo bridge to the coordinated peroxide group, results in an end-bound hydroperoxide ligand stabilized by internal hydrogen bonding.[8,13] The reversibility of this process is essential to the function of Hr. In RR, on the other hand, irreversible oxidation of the reduced form of the diiron(II) core occurs to yield an oxo-bridged diiron(III) center and a tyrosyl radical that is required for catalysis of ribonucleotide reduction.[14-22] The fate of the fourth oxidizing equivalent from O_2 remains unclear, however, and although the structure of the (μ-oxo)diiron(III) form of RR has recently been elucidated by X-ray crystallography,[22] little is known of the coordination environment about its reactive diferrous core. Even less is known about the active site of MMO, the diiron(II) form of which performs the difficult task of hydroxylating methane in the presence of O_2.[23-25]

Despite the functional importance and relative lack of structural knowledge of the diferrous forms of Hr, RR, and MMO, only two relevant model compounds containing linked Fe(II) ions were known at the outset of this work. Both $[Fe_2(OH)(O_2CCH_3)_2(Me_3TACN)_2](ClO_4)$ (**3**)[4c] and $[Fe_2(BPMP)(O_2CCH_2CH_3)_2](BPh_4)$ (BPMP = 2,6-bis[bis(2-pyridylmethyl)aminomethyl]-4-methylphenoxide) (**4**)[26] were assembled by mixing a ferrous salt and the appropriate nitrogen donor ligand with the sodium salt of a carboxylic acid in methanol under anaerobic conditions. Although **3** and **4** adequately model many of the structural and spectroscopic features of the reduced forms of the metalloproteins, they are deficient in their ability to mimic the biological activity of the protein cores. In particular, the binding and subsequent activation of dioxygen by deoxyHr and, presumably, other diiron–oxo proteins necessitates a vacant coordination position at the active site, a prerequisite precluded in **3** and **4** by the presence of tridentate, facially coordinating ligands capping their diiron(II) cores. We envisioned that, by using a bidentate terminal ligand, access to an open coordination position(s) would be afforded, a strategy that has been successfully applied to the synthesis of (μ-oxo)bis(μ-carboxylato)diiron(III) species with labile chloride groups.[3] Moreover, a ligand with imidazoles as the sole N-donor groups was sought in order more accurately to emulate the histidine ligation in the proteins. Such ligands have been used extensively to model zinc and copper sites in metalloproteins,[27] but they have been applied only rarely to model diiron centers.[2,3b]

In order to meet these objectives the target 2,2′-bis(1-methylimidazolyl)phenylmethoxymethane (BIPhMe) was designed (Scheme II). It proved to be both accessible in multigram quantities and to facilitate crystallization of reaction products for X-ray structural analysis. In the present article we report the use of BIPhMe for the self-assembly of a diiron(II) complex containing only biomimetic ligands and inherent asymmetry owing to the presence of five- and six-coordinate metal centers. In a reaction relevant to the functional activity of RR and possibly MMO, an oxygen atom from O_2 is incorporated upon exposure of the complex to air to afford a (μ-oxo)diiron(III) species. Full details of the structural, spectroscopic, and physical characterization of these complexes as well as mechanistic studies of the dioxygen activation

(6) Drüeke, S.; Wieghardt, K.; Nuber, B.; Weiss, J. *Inorg. Chem.* **1989**, *28*, 1414–1417.

(7) (a) Armstrong, W. H.; Lippard, S. J. *J. Am. Chem. Soc.* **1985**, *107*, 3730–3731. (b) Drüeke, S.; Wieghardt, K.; Nuber, B.; Weiss, J.; Fleischhauer, H.-P.; Gehring, S.; Haase, W. *J. Am. Chem. Soc.* **1989**, *111*, 8622–8631. (c) Turowski, P. N.; Armstrong, W. H.; Roth, M. E.; Lippard, S. J. *J. Am. Chem. Soc.* **1990**, *112*, 681–690.

(8) Stenkamp, R. E.; Sieker, L. C.; Jensen, L. H.; McCallum, J. D.; Sanders-Loehr, J. *Proc. Natl. Acad. Sci. U.S.A.* **1985**, *82*, 713–716.

(9) Zhang, K.; Stern, E. A.; Ellis, F.; Sanders-Loehr, J.; Shiemke, A. K. *Biochemistry* **1988**, *27*, 7470–7479.

(10) (a) Reem, R. C.; Solomon, E. I. *J. Am. Chem. Soc.* **1984**, *106*, 8323–8325. (b) Reem, R. C.; Solomon, E. I. *J. Am. Chem. Soc.* **1987**, *109*, 1216–1226.

(11) Maroney, M. J.; Kurtz, D. M., Jr.; Nocek, J. M.; Pearce, L. L.; Que, L., Jr. *J. Am. Chem. Soc.* **1986**, *108*, 6871–6879.

(12) Clark, P. E.; Webb, J. *Biochemistry* **1981**, *20*, 4628–4632.

(13) Shiemke, A. K.; Loehr, T. M.; Sanders-Loehr, J. *J. Am. Chem. Soc.* **1984**, *106*, 4951–4956.

(14) Stubbe, J. *J. Biol. Chem.* **1990**, *265*, 5329–5332.

(15) Fontecave, M.; Eliasson, R.; Reichard, P. *J. Biol. Chem.* **1989**, *264*, 9164–9170.

(16) Lynch, J. B.; Juarez-Garcia, C.; Münck, E.; Que, L., Jr. *J. Biol. Chem.* **1989**, *264*, 8091–8096.

(17) Sahlin, M.; Gräslund, A.; Petersson, L.; Ehrenberg, A.; Sjöberg, B.-M. *Biochemistry* **1989**, *28*, 2618–2625.

(18) Scarrow, R. C.; Maroney, M. J.; Palmer, S. M.; Que, L., Jr.; Roe, A. L.; Salowe, S. P.; Stubbe, J. *J. Am. Chem. Soc.* **1987**, *109*, 7857–7864.

(19) Bunker, G.; Petersson, L.; Sjöberg, B.-M.; Sahlin, M.; Chance, M.; Chance, B.; Ehrenberg, A. *Biochemistry* **1987**, *26*, 4708–4716.

(20) Atkin, C. L.; Thelander, L.; Reichard, P.; Lang, G. *J. Biol. Chem.* **1973**, *248*, 7464–7472.

(21) Petersson, L.; Gräslund, A.; Ehrenberg, A.; Sjöberg, B.-M.; Reichard, P. *J. Biol. Chem.* **1980**, *255*, 6706–6712.

(22) Nordlund, P.; Sjöberg, B.-M.; Eklund, H. *Nature* **1990**, *345*, 593–598.

(23) (a) Fox, B. G.; Froland, W. A.; Dege, J. E.; Lipscomb, J. D. *J. Biol. Chem.* **1989**, *264*, 10023–10033. (b) Fox, B. G.; Surerus, K. K.; Münck, E.; Lipscomb, J. D. *J. Biol. Chem.* **1988**, *263*, 10553–10556.

(24) (a) Green, J.; Dalton, H. *J. Biol. Chem.* **1989**, *264*, 17698–17703. (b) Ruzicka, F.; Huang, D. S.; Donnelly, M. I.; Frey, P. A. *Biochemistry* **1990**, *29*, 1696–1700.

(25) (a) Ericson, A.; Hedman, B.; Hodgson, K. O.; Green, J.; Dalton, H. D.; Bentsen, J. G.; Beer, R. H.; Lippard, S. J. *J. Am. Chem. Soc.* **1988**, *110*, 2330–2332. (b) Prince, R. C.; George, G. N.; Savas, J. C.; Cramer, S. P.; Patel, R. N. *Biochim. Biophys. Acta* **1988**, *952*, 220–229.

(26) (a) Borovik, A. S.; Que, L., Jr. *J. Am. Chem. Soc.* **1988**, *110*, 2345–2347. (b) Borovik, A. S.; Hendrich, M. P.; Holman, T. R.; Münck, E.; Papaefthymiou, V.; Que, L., Jr. *J. Am. Chem. Soc.* **1990**, *112*, 6031–6038.

(27) Selected examples: (a) Knapp, S.; Keenan, T. P.; Liu, J.; Potenza, J. A.; Schugar, H. J. *Inorg. Chem.* **1990**, *29*, 2191–2192. (b) Tolman, W. B.; Rardin, R. L.; Lippard, S. J. *J. Am. Chem. Soc.* **1989**, *111*, 4532–4533. (c) Traylor, T. G.; Hill, K. W.; Tian, Z.-Q.; Rheingold, A. L.; Peisach, J.; McCracken, J. *J. Am. Chem. Soc.* **1988**, *110*, 5571–5573. (d) Knapp, S.; Keenan, T. P.; Zhang, X.; Fikar, R.; Potenza, J. A.; Schugar, H. J. *J. Am. Chem. Soc.* **1987**, *109*, 1882–1883. (e) Sorrell, T. N.; Borovik, A. S. *J. Am. Chem. Soc.* **1987**, *109*, 4255–4260. (f) Sorrell, T. N.; Borovik, A. S. *J. Am. Chem. Soc.* **1986**, *108*, 2479–2481. (g) Slebocka-Tilk, H.; Cocho, J. L.; Frakman, Z.; Brown, R. S. *J. Am. Chem. Soc.* **1984**, *106*, 2421–2431. (h) Tang, C. C.; Davalian, D.; Huang, P.; Breslow, R. *J. Am. Chem. Soc.* **1978**, *100*, 3918–3922. (i) Clewley, R. G.; Slebocka-Tilk, H.; Brown, R. S. *Inorg. Chim. Acta* **1989**, *157*, 233–238.

reaction are described. Portions of this work were communicated previously.[28]

Experimental Section

Materials and Methods. $Fe(O_2CH)_2 \cdot 2H_2O$ was prepared according to a literature procedure.[29] Tetrahydrofuran (THF) and 1,2-dichloroethane were distilled from sodium benzophenone ketyl and CaH_2, respectively. All other reagents were obtained from commercial suppliers and used as supplied. Air-sensitive materials were handled either under N_2 in a Vacuum Atmospheres, Inc. glovebox or under Ar by using standard vacuum line techniques. ^{18}O-enriched water (99%) and dioxygen (98%) were supplied by Stohler Isotope Laboratories, Waltham, MA and Cambridge Isotope Laboratories, Woburn, MA, respectively. Mössbauer spectra of samples prepared in a BN matrix were recorded at the Francis Bitter National Magnet Laboratory as previously described.[4c] Resonance Raman spectra were obtained by using a krypton ion Innova 70 laser (406.7 nm, 75 mW) and an EG&G Princeton Applied Research optical multichannel analyzer consisting of a Model 1460 system processor and a Model 1455 photodiode array detector. ^1H-NMR spectra and T_1 measurements were obtained on either Varian XL 300 or Bruker WM 250 or AC 250 instruments; chemical shifts were referenced to internal tetramethylsilane. Electronic and Fourier transform infrared spectroscopic measurements were obtained on Varian Lambda 7 and Mattson Cygnus 400 instruments, respectively.

2,2′-Bis(1-methylimidazolyl)phenylhydroxymethane (BIPhOH). To a solution of 1-methylimidazole (23.9 mL, 0.30 mol) in THF (500 mL) at −78 °C under Ar was added BuLi (130.0 mL, 2.3 M) dropwise over 45 min. After stirring an additional 15 min, benzoyl chloride (17.4 mL, 0.15 mol) was added, and the resulting dark brown mixture was allowed to warm to room temperature. Brine (300 mL) was added, and the solution was extracted with CH_2Cl_2 (3 × 200 mL). The combined extracts were dried over Na_2CO_3, solvent was removed under reduced pressure, and the residue was triturated with Et_2O (3 × 40 mL). The resulting white powder (33.0 g, 82%) was used directly to prepare BIPhMe. Analytically pure colorless blocks of BIPhOH could be obtained by crystallization of the powder from boiling benzene: mp 170–171 °C; ^1H NMR ($CDCl_3$, 250 MHz) δ 3.39 (s, 6 H), 6.66 (br s, 1 H), 6.88 (unresolved doublet, 2 H), 6.94 (unresolved doublet, 2 H), 7.09 (m, 2 H), 7.34 (m, 3 H); FTIR (KBr, cm^{-1}) 3310, 3106, 2952, 1527 (w), 1483, 1450, 1407 (w), 1353, 1280, 1174, 1143, 1088, 1058, 937, 886, 753, 716, 686, 638, 609, 576. Anal. Calcd for $C_{15}H_{16}N_4O$: C, 67.15; H, 6.01; N, 20.88. Found: C, 67.29; H, 6.03; N, 20.85.

2,2′-Bis(1-methylimidazolyl)phenylmethoxymethane (BIPhMe). To a slurry of BIPhOH (33.0 g, 0.123 mol) in THF (400 mL) was added powdered KOH (14 g, 0.25 mol). After stirring the mixture vigorously for 15 min, CH_3I (15.5 mL, 0.25 mol) was added, and stirring was continued for 10 h. Brine (200 mL) was added, and the resulting solution was extracted with CH_2Cl_2 (3 × 200 mL). After drying the combined extracts over Na_2CO_3, solvent was removed under reduced pressure, and the resulting residue was crystallized from boiling acetone (~250 mL) to give BIPhMe as colorless prisms (23.4 g, 67%). Samples of BIPhMe containing deuterium in the *O*-methyl and/or *N*-methyl groups were prepared via analogous procedures by using CD_3I instead of CH_3I where appropriate: mp 179–180 °C; ^1H NMR ($CDCl_3$, 250 MHz) δ 3.26 (s, 3 H), 3.45 (s, 6 H), 6.84 (d, J = 1.0 Hz, 2 H), 7.00 (d, J = 1.0 Hz, 2 H), 7.32 (br m, 3 H), 7.52 (br m, 2 H); FTIR (KBr, cm^{-1}) 3092, 2939, 2827 (w), 1488, 1449, 1402 (w), 1282, 1183 (w), 1135 (w), 1062, 974, 896, 767, 727, 705 (w), 684 (w), 651 (w). Anal. Calcd for $C_{16}H_{18}N_4O$: C, 68.06; H, 6.43; N, 19.84. Found: C, 68.28; H, 6.46; N, 19.97.

$[Fe_2(O_2CH)_4(BIPhMe)_2]$ (1). (Note: all manipulations must be performed in the strict absence of air). A mixture of BIPhMe (0.312 g, 1.11 mmol) and $Fe(O_2CH)_2 \cdot 2H_2O$ (0.200 g, 1.10 mmol) in 15.0 mL of MeOH was stirred under Ar for 1 h. Solvent was removed from the clear, pale green solution under vacuum, and the residue was extracted with CH_2Cl_2 (~8 mL) and filtered. The volume of the filtrate was reduced to 4–5 mL, CH_3CN (~5 mL) was added, and the solution was stored at −20 °C for 4 days. The resulting pale green (almost colorless) crystals that deposited were collected, washed with CH_3CN (2 × 2 mL), and dried under vacuum (404 mg, 86%). Crystals of $1 \cdot CHCl_3 \cdot CH_3CN$ suitable for X-ray diffraction studies were obtained in a similar manner by using $CHCl_3$ instead of CH_2Cl_2: FTIR (KBr, cm^{-1}) 3122, 2955, 2940, 1609 (s). 1498, 1449, 1358, 1323, 1283, 1071, 988, 897, 762, 725, 702; UV–vis (CH_2Cl_2) [λ_{max}, nm (ϵ_M/Fe cm^{-1} M^{-1})] 290 (200). Anal. Calcd for $C_{36}H_{40}N_8O_{10}Fe_2$: C, 50.49; H, 4.71; N, 13.08; Fe, 13.04. Found: C, 50.20; H, 4.61; N, 13.01; Fe, 12.65.

$[Fe_2O(O_2CH)_4(BIPhMe)_2] \cdot H_2O$ ($2 \cdot H_2O$). The reaction of BIPhMe and $Fe(O_2CH)_2 \cdot 2H_2O$ was performed under Ar as described for the preparation of **1**, except that, after removing solvent from the reaction mixture, the residue was extracted with $CHCl_3$ (5 mL) and exposed to air, and the resulting deep brown-green solution was filtered. Addition of CH_3CN (5 mL) followed by slow evaporation afforded green crystals of $2 \cdot H_2O$ as thin green plates (0.431 g, 88%). Air oxidation of $CHCl_3$ solutions of purified **1** gave similar yields of $2 \cdot H_2O$. Crystals of $2 \cdot 2CH_3OH \cdot H_2O$ suitable for X-ray crystallographic analysis were grown by slow evaporation of a CH_3OH solution: FTIR (KBr, cm^{-1}) 3424, 3130, 2937, 2832, 1617 (sh), 1590 (s), 1500, 1449, 1356, 1310, 1283, 1070, 988, 900, 762, 725, 704. Anal. Calcd for $C_{36}H_{42}N_8O_{12}Fe_2$: C, 48.56; H, 4.75; N, 12.58. Found: C, 48.51; H, 4.78; N, 12.51. Samples of $2 \cdot H_2O$ for resonance Raman spectroscopic measurements were prepared in $CHCl_3/CH_3OH$ (~20:1; ~6 mM). ^{18}O-labeled $2 \cdot H_2O$ was prepared by two methods. In one, an excess of $^{18}O_2$ was admitted to an evacuated flask containing a rapidly stirred solution of **1** in $CHCl_3$ (6.0 mM) at room temperature. The initially colorless solution immediately turned deep green. After ~5 min, the solution was freeze–pump–thaw degassed, removed to a glovebox, and transferred to an NMR tube for resonance Raman spectroscopic monitoring. Alternatively, the ^{18}O-labeled complex was prepared by adding $H_2{}^{18}O$ (~100 μL; ~7 equiv) to a solution of $2 \cdot H_2O$ in an NMR tube followed by rapid mixing for ~10 min before acquisition of resonance Raman spectra.

$[Zn(BIPhMe)Cl_2]$ (6). To a solution of anhydrous $ZnCl_2$ (0.050 g, 0.37 mmol) in 1.0 mL of MeOH was added a solution of BIPhMe (0.104 g, 0.37 mmol) in 2.0 mL of MeOH. A white, microcrystalline precipitate formed immediately and was collected, washed with MeOH (2 × 1 mL) and Et_2O (1 × 3 mL), and dried under vacuum (0.141 g, 91%): ^1H NMR (CD_3CN, 300 MHz) δ 3.16 (s, 3 H), 3.55 (s, 6 H), 7.16 (d, J = 1.4 Hz, 2 H), 7.19 (d, J = 1.4 Hz, 2 H), 7.3–7.45 (m, 3 H), 7.6 (m, 2 H); FTIR (KBr, cm^{-1}) 3142, 3116, 2954, 1636 (w), 1605 (w), 1545 (w), 1503, 1476, 1447, 1403, 1288, 1179, 1156, 1071, 992, 899, 763, 727, 701. Anal. Calcd for $C_{16}H_{18}N_4OCl_2Zn$: C, 45.91; H, 4.33; N, 13.38; Cl, 16.94. Found: C, 46.14; H, 4.36; N, 13.46; Cl, 17.02.

X-ray Crystallography. A colorless block-shaped crystal of $1 \cdot CHCl_3 \cdot CH_3CN$ (dimensions 0.40 × 0.30 × 0.15 mm), a green plate-shaped crystal of $2 \cdot 2CH_3OH \cdot H_2O$ (dimensions 0.25 × 0.15 × 0.05 mm), and a colorless plate-shaped crystal of **6** (dimensions 0.15 × 0.30 × 0.30 mm) were mounted on glass fibers either with silicon grease on a cold stage (**1**) or with epoxy resin (**2** and **6**). Relevant crystallographic information is presented in Table I. Unit cell parameters and intensity data were obtained by using the general procedures previously described.[30] Corrections were applied for Lorentz and polarization effects, but it was unnecessary to account for crystal decay. An empirical absorption correction was applied to the data for $2 \cdot 2CH_3OH \cdot H_2O$ but not to the data for $1 \cdot CHCl_3 \cdot CH_3CN$ or **6**. The structures of the compounds were solved by using the direct methods program MITHRIL and standard difference Fourier methods in the TEXSAN package.[31] The positions of all non-hydrogen atoms were refined with anisotropic thermal parameters, and the H atom positions were placed at calculated positions for the final refinement cycles. The largest peak in the final difference Fourier map for $1 \cdot CHCl_3 \cdot CH_3CN$ had 0.8 $e^-/Å^3$ and was located near Cl3 of the $CHCl_3$ solvent molecule. For $2 \cdot 2CH_3OH \cdot H_2O$, the maximum residual electron density of 0.4 $e^-/Å^3$ was located near Fe1, and for **6** it was 0.5 $e^-/Å^3$ located near Zn. Selected bond distances and angles for $1 \cdot CHCl_3 \cdot CH_3CN$ and $2 \cdot 2CH_3OH \cdot H_2O$ are provided in Table II. Full listings of bond distances and angles for all three complexes may be found in supplementary material Tables S1–S6. Positional parameters and B(eq) for all atoms are supplied in Tables S7–S9, final thermal parameters for all non-hydrogen atoms are given in Tables S10–S12, and listings of observed and calculated structure factor amplitudes may be found in Tables S13–S15.

Magnetic Susceptibility Measurements. Solid-state magnetic susceptibilities of 38.3 mg of powdered **1** in a polyethylene sample container and 18.7 mg of powdered $2 \cdot H_2O$ in an Al–Si sample container were measured by using an S.H.E. Model 905 SQUID susceptometer at the Francis Bitter National Magnet Laboratory. A total of 44 data points was taken for each sample at a field of 10 kG over the temperature range 6.0–300 K. In addition, measurements of the susceptibility of **1** in fields ranging from 1.0 to 50 kG were collected at 6.0, 80, and 300 K. The susceptibilities of the sample holders used in the experiments were measured at the same temperatures and fields to allow subtraction of their paramagnetic contributions to the total susceptibilities. Diamag-

(28) Tolman, W. B.; Bino, A.; Lippard, S. J. *J. Am. Chem. Soc.* **1989**, *111*, 8522–8523.

(29) (a) Rhoda, R. N.; Fraioli, A. V. *Inorg. Synth.* **1953**, *4*, 159–161. (b) Weber, G. *Acta Crystallogr.* **1980**, *B36*, 3107–3109.

(30) Silverman, L. D.; Dewan, J. C.; Giandomenico, C. M.; Lippard, S. J. *J. Inorg. Chem.* **1980**, *19*, 3379–3383.

(31) TEXRAY Structure Analysis Package, Molecular Structure Corporation, College Station TX, 1985.

Table I. Crystallographic Information for $[Fe_2(O_2CH)_4(BIPhMe)_2]\cdot CHCl_3\cdot CH_3CN$ (**1**·$CHCl_3$·CH_3CN), $[Fe_2O(O_2CH)_4(BIPhMe)_2]\cdot 2CH_3OH\cdot H_2O$ (**2**·$2CH_3OH$·H_2O), and $[Zn(BIPhMe)Cl_2]$ (**6**)

	1·$CHCl_3$·CH_3CN	**2**·$2CH_3OH$·H_2O	**6**
formula	$C_{39}H_{44}N_9O_{10}Cl_3Fe_2$	$C_{38}H_{50}N_8O_{14}Fe_2$	$C_{16}H_{18}N_4OCl_2Zn$
formula wt, g mol^{-1}	1016.9	954.6	418.6
space group	$P\bar{1}$	$P\bar{1}$	$P2_1/n$
a, Å	15.396 (2)	15.203 (2)	10.262 (2)
b, Å	15.985 (1)	15.374 (1)	14.089 (2)
c, Å	10.637 (1)	10.163 (1)	13.274 (2)
α, deg	98.937 (8)	108.175 (8)	90
β, deg	105.328 (8)	96.32 (1)	104.14 (2)
γ, deg	63.024 (8)	74.244 (9)	90
V, Å^3	2248.1 (9)	2171.2 (4)	1861 (1)
Z	2	2	4
D_{calcd}, g cm^{-1}	1.502	1.460	1.494
D_{obsd},[a] g cm^{-1}		1.44 (1)	
temp, K	194	194	217
radiation	Mo Kα (0.71073 Å)	Mo Kα (0.71073 Å)	Mo Kα (0.71073 Å)
abs coeff, cm^{-1}	8.9	7.4	16.5
min trans. coeff[c]	0.96	0.91	0.86
data collected	$3° \le 2\theta \le 50°$, +h, ±k, ±l	$3° \le 2\theta \le 45°$, +h, ±k, ±l	$3° \le 2\theta \le 48°$, ±h, +k, +l
total no. of data collected	8212	5905	3370
total no. of unique data	7566	5646	2385
no. of unique data with $I > 3\sigma(I)$	5983	3525	2270[d]
no. of variable parameters	568	559	217
R_1[b]	0.041	0.055	0.035
R_2[b]	0.057	0.064	0.048

[a] Measured at room temperature by suspension in a mixture of MeI and heptane. [b] $R_1 = \sum||F_o| - |F_c||/\sum|F_o|$; $R_2 = |\sum w||F_o| - |F_c||^2/\sum w|F_o|^2]^{1/2}$, where $w = 1/\sigma^2(F_o)$ and $\sigma^2(F_o^2) = [S^2(C + R^2B) + (pF_o^2)^2]/Lp^2$ with S = scan rate, C = peak count, B = background, R = scan-to-background time ratio, Lp = Lorentz-polarization factor, and p = fudge factor, set to 0.05. [c] Maximum transmission coefficient normalized to 1.0. [d] $I > 6\sigma(I)$.

Table II. Selected Interatomic Distances (Å) and Angles (deg) for $[Fe_2(O_2CH)_4(BIPhMe)_2]\cdot CHCl_3\cdot CH_3CN$ (**1**·$CHCl_3$·CH_3CN) and $[Fe_2O(O_2CH)_4(BIPhMe)_2]\cdot 2CH_3OH\cdot H_2O$ (**2**·$2CH_3OH$·H_2O)[a]

1				**2**			
Fe1···Fe2	3.5736 (8)			Fe1···Fe2	3.211 (2)		
Fe1–O1	2.172 (2)	Fe2–O1	2.113 (2)	Fe1–O	1.801 (5)	Fe2–O	1.793 (4)
Fe1–O4	2.162 (2)	Fe2–O3	2.094 (2)	Fe1–O3	2.013 (5)	Fe2–O1	2.033 (5)
Fe1–O6	2.150 (2)	Fe2–O5	2.039 (3)	Fe1–O6	2.062 (5)	Fe2–O5	2.104 (5)
Fe1–O2	2.062 (2)	Fe2–N31	2.109 (3)	Fe1–O8	2.115 (5)	Fe2–O7	2.070 (5)
Fe1–N11	2.142 (3)	Fe2–N41	2.133 (3)	Fe1–N11	2.117 (6)	Fe2–N31	2.114 (6)
Fe1–N21	2.145 (3)			Fe1–N21	2.152 (6)	Fe2–N41	2.187 (6)
O1–C3	1.270 (4)	O7–C3	1.214 (4)	O1–C6	1.234 (9)	O2–C6	1.237 (9)
O2–C6	1.257 (4)	O8–C6	1.224 (4)	O3–C5	1.270 (9)	O4–C5	1.210 (9)
O3–O5	1.257 (4)	O4–C5	1.233 (4)	O5–C3	1.250 (8)	O6–C3	1.244 (9)
O5–C4	1.256 (4)	O6–C4	1.229 (4)	O7–C4	1.250 (9)	O8–C4	1.238 (9)
O1–Fe1–O2	171.6 (1)	O1–Fe2–O3	88.8 (1)	O–Fe1–O3	98.1 (2)	O–Fe2–O1	96.4 (2)
O1–Fe1–O4	85.2 (1)	O1–Fe2–O5	108.5 (1)	O–Fe1–O6	96.8 (2)	O–Fe2–O5	93.9 (2)
O1–Fe1–O6	86.0 (1)	O1–Fe2–N31	146.7 (1)	O–Fe1–O8	94.7 (2)	O–Fe2–O7	97.6 (2)
O1–Fe1–N11	91.1 (1)	O1–Fe2–N41	90.3 (1)	O–Fe1–N11	92.8 (2)	O–Fe2–N31	93.8 (2)
O1–Fe1–N21	92.9 (1)	O3–Fe2–O5	94.0 (1)	O–Fe1–N21	173.8 (2)	O–Fe2–N41	172.5 (2)
O2–Fe1–O4	88.5 (1)	O3–Fe2–N31	92.4 (1)	O3–Fe1–O6	88.9 (2)	O1–Fe2–O5	169.7 (2)
O2–Fe1–O6	88.7 (1)	O3–Fe2–N41	173.2 (1)	O3–Fe1–O8	166.5 (2)	O1–Fe2–O7	89.0 (2)
O2–Fe1–N11	94.8 (1)	O5–Fe2–N31	104.5 (1)	O3–Fe1–N11	93.5 (2)	O1–Fe2–N31	86.9 (2)
O2–Fe1–N21	93.7 (1)	O5–Fe2–N41	92.7 (1)	O3–Fe1–N21	85.5 (2)	O1–Fe2–N41	89.7 (2)
O4–Fe1–O6	92.6 (1)	N31–Fe2–N41	84.6 (1)	O6–Fe1–O8	85.3 (2)	O5–Fe2–O7	89.3 (2)
O4–Fe1–N11	93.0 (1)	Fe1–O1–Fe2	113.0 (1)	O6–Fe1–N11	169.7 (2)	O5–Fe2–N31	92.7 (2)
O4–Fe1–N21	176.3 (1)			O6–Fe1–N21	88.3 (2)	O5–Fe2–N41	80.1 (2)
O6–Fe1–N11	173.5 (1)			O8–Fe1–N11	90.2 (2)	O7–Fe2–N31	168.3 (2)
O6–Fe1–N21	90.4 (1)			O8–Fe1–N21	82.2 (2)	O7–Fe2–N41	86.8 (2)
N11–Fe1–N21	83.9 (1)			N11–Fe1–N21	81.9 (2)	N31–Fe2–N41	82.2 (2)
				Fe1–O–Fe2	126.6 (1)		

	min	max	mean	min	max	mean
O–C	1.410 (4)	1.437 (5)	1.424	1.42 (1)	1.43 (1)	1.425
C1–C2–C_{ring}	1.521 (4)	1.546 (4)	1.530	1.51 (1)	1.55 (1)	1.530
C–C_{phenyl}	1.376 (6)	1.395 (5)	1.384	1.35 (1)	1.40 (1)	1.381
C–C_{imid}	1.342 (5)	1.356 (5)	1.347	1.33 (1)	1.36 (1)	1.343
N–$C_{imid\ ring}$	1.318 (4)	1.381 (4)	1.358	1.317 (9)	1.389 (9)	1.359
N–C_{methyl}	1.460 (4)	1.470 (4)	1.466	1.45 (1)	1.47 (1)	1.468

[a] See Figures 1 and 2 for labeling schemes. Estimated standard deviations, in parentheses, occur in the last significant digit. No corrections were made for thermal motion.

netic corrections of -458×10^{-6} emu G^{-1} mol^{-1} for **1** and -482×10^{-6} emu G^{-1} mol^{-1} for **2**·H_2O were calculated by using Pascal's constants.[32] The data were fit to the appropriate theoretical expressions, the Curie–Weiss equation or the expression derived from the general isotropic ex-

change Hamiltonian $\mathcal{H} = -2JS_1 \cdot S_2$, where $S_1 = S_2 = 2$ for **1** and $S_1 = S_2 = {}^5/_2$ for **2**·H_2O as described in ref 4c and 32, by a nonlinear least-squares method with the use of locally written programs.[33] For **1**, plots of the observed moments versus field were linear below 15 kG between 6 and 300 K, indicating that the variable-temperature data collected at 10 kG is not significantly perturbed by saturation effects.

Electron Paramagnetic Resonance Experiments. EPR spectra were recorded with a Bruker Model ESP 300 spectrometer fitted with an Oxford Instruments, Inc. liquid helium cryostat. Diphenylpicrylhydrazyl or an aqueous solution of $MnSO_4$ was used as calibrant. Integrations were performed by using a standard solution that contained $CuSO_4$ (0.9730 mM), $NaClO_4$ (2 M), HCl (0.1 M), and 20% glycerol. All samples were prepared by first dissolving **1** in CH_2Cl_2 in a glovebox (stock solution volumes 5.0–10.0 mL, concentrations 1.7–5.5 mM) followed by transfer to 3-mm diameter quartz tubes. Sample solutions were then either immediately sealed and frozen by immersion in liquid nitrogen or were first exposed to air as described in the text and then frozen. For power saturation experiments, the temperature of the sample solution was determined by calibration under identical helium flow conditions with a carbon resistor immersed in an equal volume of ethylene glycol. Power saturation data were collected at temperatures between 8.2 and 13.8 K by measuring signal intensities (peak-to-peak heights) as a function of microwave power. The half saturation power, $P_{1/2}$, at each temperature was determined by graphical methods.[34]

Manometry. The quantity of dioxygen consumed in the conversion of **1** to **2** was measured by using a locally constructed apparatus consisting of a mercury U-tube opened at one end to the atmosphere and branched at the other, with a Teflon stopcock at each branch. One arm was attached to a dual manifold vacuum line, and the other was fitted with an O-ring joint for connection to the reaction flask, an ~10-mL vessel fitted with a Teflon stopper and a sidearm with an O-ring joint. In a typical experiment, a mixture of partially dissolved **1** (102 mg, 1.19 mmol) in 1,2-dichloroethane (7.0 mL) was loaded into the reaction flask in the glovebox, the flask was sealed and attached to the apparatus via the O-ring joint, the mixture was freeze–pump–thaw degassed (two cycles), and the Teflon valve between the flask and the apparatus was closed. After complete evacuation of the apparatus, O_2 was added via the double manifold, the Teflon valve to the manifold was closed, and the Teflon valve to the flask was opened to allow the oxidation reaction to proceed. The solution was rapidly stirred at 297 K (variation was <1 K over the time of the experiment) for 0.5 h, at which time all of the material had dissolved, and the solution was dark green-brown. After standing for 1.5 h to allow complete equilibration (no change in pressure), a pressure reading was taken. Subtraction of this final reading from that of a control experiment in which the above procedure was repeated by using solvent only (identical volume, temperature, equilibration time, and initial O_2 pressure) gave the pressure difference incurred by dioxygen uptake. Prior calibration of the system by using known quantities of gas allowed conversion of this pressure difference to mols of O_2 (in this instance, 0.7 mmol or 0.6 equiv). Three replicate measurements using similar amounts of starting material were performed, the result being 0.6 ± 0.1 equiv of O_2 consumed per mol of **1**. While UV–vis spectra of the final solutions clearly indicated predominant formation of **2**, the presence of a small amount of another species was evident (shoulder at ~540 nm).

Results and Discussion

Syntheses. The ligand BIPhMe can be routinely and reproducibly synthesized in 50–55% overall yield on a >20-g scale as described in Scheme II, a route analogous to those developed for other polyimidazole ligands.[27b,e–h] Both the isolable intermediate BIPhOH and BIPhMe were characterized by elemental analysis and ^{1}H NMR and FTIR spectroscopy.

Treatment of $Fe(O_2CH)_2 \cdot 2H_2O$ with an equimolar quantity of BIPhMe in methanol under argon gave a pale green solution that, after workup, afforded $[Fe_2(O_2CH)_4(BIPhMe)_2]$ (**1**) as colorless to pale green crystals in 86% yield (eq 1). Interestingly, a similar procedure wherein $Fe(O_2CCH_3)_2$ was used instead of ferrous formate yielded only the trinuclear complex $[Fe_3(O_2CCH_3)_6(BIPhMe)_2]$ (**5**), with no evidence for the acetate-bridged dinuclear analogue of **1**.[35]

$$Fe(O_2CH)_2 \cdot 2H_2O + BIPhMe \xrightarrow[Ar]{MeOH} \underset{(\mathbf{1})}{[Fe_2(O_2CH)_4(BIPhMe)_2]} \quad (1)$$

Complex **1** is exceedingly air sensitive, especially in solution. Exposure of a $CHCl_3$ or CH_2Cl_2 solution of **1** to air at room temperature caused an immediate darkening to green-brown of the initially colorless solution. Monitoring of the reaction solution by UV–vis spectroscopy revealed formation predominantly (ca. >90%) of $[Fe_2O(O_2CH)_4(BIPhMe)_2]$ (**2**), although broad absorptions due to an uncharacterized brown species were observed, indicating that formation of **2** was not quantitative. Nonetheless, subsequent addition of CH_3CN induced crystallization of **2**·H_2O in 88% isolated yield (eq 2). Alternatively, **2**·H_2O could be prepared by stirring an equimolar mixture of $Fe(O_2CH)_2 \cdot 2H_2O$ and BIPhMe in $CHCl_3/CH_3CN$ in air, albeit in lower yield (~35%).

The complex $[Zn(BIPhMe)Cl_2]$ (**6**), used as a diamagnetic analogue for calibration of ligand ^{1}H-NMR chemical shifts, was isolated from the reaction of anhydrous $ZnCl_2$ with BIPhMe in methanol in 92% yield (eq 3).

$$\underset{(\mathbf{1})}{[Fe_2(O_2CH)_4(BIPhMe)_2]} \xrightarrow{O_2} \underset{(\mathbf{2}\cdot H_2O)}{[Fe_2O(O_2CH)_4(BIPhMe)_2] \cdot H_2O} \quad (2)$$

$$ZnCl_2 + BIPhMe \xrightarrow{MeOH} \underset{(\mathbf{6})}{[Zn(BIPhMe)Cl_2]} \quad (3)$$

X-ray Crystallography. ORTEP representations of the structures of **1**·$CHCl_3$·CH_3CN and **2**·$2CH_3OH$·H_2O are shown in Figures 1 and 2, respectively, and selected interatomic distances and angles for both molecules are listed in Table II. Both crystal structures were redetermined since the previous preliminary communication[28] to yield more precise geometrical parameters. In the case of **1**, higher quality crystals were obtained by allowing a mixed $CHCl_3/CH_3CN$ (instead of CH_2Cl_2/CH_3CN) solution to stand at −20 °C, whereas the same crystallization method was used for **2** as previously reported.

$[Fe_2(O_2CH)_4(BIPhMe)_2] \cdot CHCl_3 \cdot CH_3CN$ (1·$CHCl_3$·CH_3CN). Complex **1** contains two ferrous ions linked by one monodentate and two bidentate (syn–syn) bridging formates. This bridging arrangement is unprecedented in diiron chemistry and represents a significant departure from the known carboxylate supported μ-oxo, μ-hydroxo, and μ-phenoxo binding modes.[2-5,26,36-38] Similar monodentate carboxylate-bridged structures have been reported for polynuclear complexes of other divalent metals[35,39,40] as well as for a diferric compound in which the carboxylate is tethered to a macrocyclic ligand.[41] Terminal ligation to the $\{Fe_2(O_2CH)_3\}^+$ core in **1** is asymmetric, with the imidazoles from one BIPhMe and a fourth monodentate formate coordinated to one iron atom (Fe1) and only two imidazoles from a second BIPhMe bound to the other (Fe2). The terminal formate binds to Fe1 via its less basic anti electron lone pair, an interesting departure from the more common attachment of metal ions to carboxylates at the syn position.[42] While the coordination of Fe1 is close to octa-

(32) (a) Carlin, R. L. In *Magnetochemistry*; Springer-Verlag: New York, 1986; pp 3–33. (b) O'Connor, C. J. *Prog. Inorg. Chem.* **1982**, *29*, 203–283.
(33) Karlin, K., Ph.D. Dissertation, Columbia University, 1975.
(34) Yim, M. B.; Kuo, L. C.; Makinen, M. W. *J. Magn. Reson.* **1982**, *46*, 247–256.
(35) Rardin, R. L.; Bino, A.; Poganiuch, P.; Tolman, W. B.; Liu, S.; Lippard, S. J. *Angew. Chem., Int. Ed. Engl.* **1990**, *29*, 812–814.
(36) Chaudhuri, P.; Wieghardt, K.; Nuber, B.; Weiss, J. *Angew. Chem., Int. Ed. Engl.* **1985**, *24*, 778–779.
(37) Snyder, B. S.; Patterson, G. S.; Abrahamson, A. J.; Holm, R. H. *J. Am. Chem. Soc.* **1989**, *111*, 5214–5223, and references therein.
(38) (a) Murch, B. P.; Bradley, F. C.; Que, L., Jr. *J. Am. Chem. Soc.* **1986**, *108*, 5027–5028. (b) Borovik, A. S.; Murch, B. P.; Que, L., Jr. *Ibid.* **1987**, *109*, 7190–7191. (c) Borovik, A. S.; Papaefthymiou, V.; Taylor, L. F.; Anderson, O. P.; Que, L., Jr. *Ibid.* **1989**, *111*, 6183–6195.
(39) Review: Rardin, R. L.; Tolman, W. B.; Lippard, S. J. Submitted for publication.
(40) Some representative examples: (a) Clegg, W.; Hunt, P. A.; Straughan, B. P.; Antonia Mendiola, M. *J. Chem. Soc., Dalton Trans.* **1989**, 1127–1131. (b) Christou, G.; Perlepes, S. P.; Libby, E.; Folting, K.; Huffman, J. C.; Webb, R. J.; Hendrickson, D. N. *Inorg. Chem.* **1990**, *29*, 3657–3666. (c) Catterick, J.; Thornton, P. *J. Chem. Soc., Dalton Trans.* **1976**, 1634–1640.
(41) Spartalian, K.; Bonadies, J. A.; Carrano, C. J. *Inorg. Chim. Acta* **1988**, *152*, 135–138.

Table III. Comparison of Structural, Mössbauer, and Magnetic Features of Carboxylate-Bridged Polyiron(II) Compounds and Selected Metalloproteins

compd	Fe–O_b,[a] Å	Fe···Fe, Å	Fe–O_b–Fe, deg	O_b–Fe–N,[b] deg	δ, mm/s	ΔE_Q, mm/s	$-J$,[c] cm^{-1}	ref
1	2.113 (2)	3.5736 (8)	113.0 (1)	146.7 (1)	1.26	2.56	~0	this work
	2.172 (2)				1.25	3.30		
3	1.987 (8)	3.32 (1)	113.2 (2)	174.2 (7)	1.16	2.83	13.1	4c
4	2.052 (1)	3.348 (1)	108.93 (6)	160.94 (6)	1.20	2.72		26
	2.062 (1)			161.32 (6)				
5	2.027 (3)	3.325 (1)	105.4 (1)	124.6 (1)	1.36	2.64	<0	35
	2.151 (3)				1.14	3.60		
deoxyHr	1.98	3.57	128		1.14	2.76	~15	8–12
RR (reduced)					1.26	3.13	~5	16, 17
MMO (reduced)					1.30	3.14		23

[a] O_b refers to the bridging oxygen atom. [b] O_b–Fe–N refers to the angle between the bridging oxygen atom and the terminal nitrogen atom in the equatorial plane (e.g., the angle O1–Fe2–N31 in **1**). [c] From temperature dependent magnetic susceptibility studies for the model compounds, from MCD–EPR (ref 10) and NMR (ref 11) for deoxyHr, and from NMR for reduced RR (ref 17).

hedral, the largest deviation from the idealized 90° angles being 6°, Fe2 has trigonal-bipyramidal geometry, highly distorted within the equatorial plane (O1, N31, and O5).[43] This distortion arises from bending of the monodentate bridging formate toward Fe2 (cf. ∠Fe1–O1–C3 = 132.1 (2)° with ∠Fe2–O1–C3 = 107.2 (2)°) and a resulting interaction of Fe2 with the "dangling" formate oxygen (Fe2···O7 = 2.787 (3) Å). A consequence of this interaction is substantial deviation of the equatorial bond angles about Fe2 from idealized 120° values. Thus, the O1–Fe2–N31 angle increases to 146.7 (1)° and the O5–Fe2–N31 and O1–Fe2–O5 angles correspondingly decrease to 104.5 (1)° and 108.5 (1)°, respectively. Despite its effects on intraligand angles about Fe2, however, the Fe2···O7 distance is significantly longer than expected for a normal Fe(II)–O bond (2.0–2.2 Å) and is therefore most consistent with, at best, a rather weak bonding interaction. In support of this interpretation, the average metal–ligand bond lengths are significantly shorter for Fe2 than for Fe1, as anticipated for a lower overall coordination number for the former (Fe2–O_{av} = 2.082 Å, Fe1–O_{av} = 2.137 Å; Fe2–N_{av} = 2.121 Å, Fe1–N_{av} = 2.144 Å). Moreover, the Fe2–N31 distance is significantly shorter than that of Fe2–N41, as expected for equatorial versus axial bond lengths in a trigonal bipyramid.[43]

It is instructive to compare the geometry of the dinuclear core of **1** to that of the analogous fragments in the acetate-bridged trinuclear complex **5** (Table III).[35] To facilitate this comparison, the structure of **5** is sketched below. Although the topological

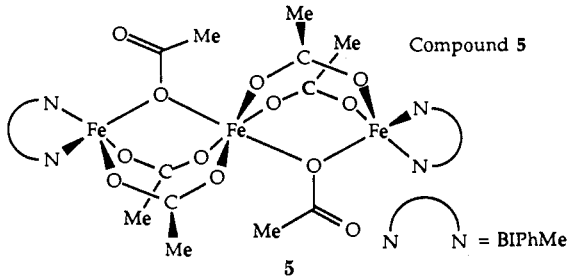

5

arrangement of the carboxylates spanning the ferrous ions is essentially the same in both compounds, there are substantial differences between the geometries of their monodentate bridging carboxylates that have important structural and physicochemical consequences (vide infra). Most significantly, the degree of interaction of the "dangling" carboxylate oxygen in **5** is less than in **1**, as revealed by a longer Fe···$O_{dangling}$ distance of 3.005 (4) Å and equatorial intraligand angles for the trigonal-bipyramidal iron atom that more closely approach 120° in **5** (124.6 (1)°, 124.9 (1)°, and 110.5 (1)°).[35] In addition, the Fe···Fe distance is shorter by 0.25 Å, and the Fe–O_b–Fe angle is smaller by 7.6° in **5** compared to **1**. Overall, these data illustrate the flexibility of the monodentate carboxylate bridge in supporting differing diiron core geometries, a feature which may have implications for understanding the structures and physical properties of the reduced forms of diiron protein active sites.[39]

Further structural comparisons among **1**, the other two known diferrous model compounds **3** and **4**, and the reduced forms of Hr, RR, and MMO are presented in Table III. Consistent with the order of basicity of the bridging ligands in the dinuclear complexes, the average Fe–O_b bond lengths increase according to hydroxo < phenoxo < formato. The Fe···Fe distance in **1** is the longest among the diiron(II) model compounds and agrees surprisingly well with the corresponding distance determined for deoxyHr by EXAFS measurements.[9] Comparison of **1** to **3**, which has a similar Fe–O_b–Fe angle but shorter Fe–O_b bond lengths, suggests that the large Fe···Fe distance in **1** arises from its long Fe–O_b distances. In deoxyHr, on the other hand, which has Fe–O_b bond lengths that closely agree with those of similarly hydroxo-bridged **3**, an acute Fe–O_b–Fe angle of 128° provides the basis for its long Fe···Fe distance.

The most important similarity between **1** and deoxyHr is the presence in both of five- and six-coordinate ferrous centers, key structural features for the proposed mechanism of dioxygen binding in the natural system (Scheme I). Oxo-bridged diiron(III) complexes containing differing coordination numbers have been prepared, but none contain additional supporting carboxylate ligands known to exist in the protein.[44] Asymmetric disposition of terminal ligands in a diiron(III) complex also has been reported, but the compound contains two six-coordinate metal centers.[5b,c] Similarities also exist between **1** and metHr, which, notwithstanding its higher oxidation state and the presence of an oxo bridge, has a pentacoordinate iron center with trigonal-bipyramidal geometry nearly congruent with that of **1**.[45] Both systems are almost identically distorted in the equatorial plane, as indicated, for example, by O_b–Fe–N angles of 146.7 (1)° for **1** and 143° for metHr. While this distortion is due to the additional interaction of the iron center with the "dangling" formate oxygen in **1**, protein constraints are presumably responsible for the irregular geometry in the natural system. A similarly distorted ligand arrangement has been suggested for deoxyHr on the basis of difference electron density maps, but the low resolution of the data (3.0 Å)[8] precludes definitive structural comparisons.

The diiron(II) cores of the reduced forms of RR and MMO are poorly characterized compared to the active site of deoxyHr, thus making **1** a potentially useful speculative model. The possibility of a monodentate carboxylate-bridged center in reduced RR is particularly intriguing, especially in light of the carboxylate-rich coordination sphere recently identified by X-ray crystallography for the (μ-oxo)diiron(III) form of the protein.[22] This idea, which is supported by analogies between the physical

(42) Carrell, C. J.; Carrell, H. L.; Erlebacher, J.; Glusker, J. P. *J. Am. Chem. Soc.* **1988**, *110*, 8651–8656, and references cited therein.
(43) Kepert, D. L. *Inorganic Stereochemistry*; Springer-Verlag: Berlin, 1982; Chapters 4 and 5.
(44) (a) Gomez-Romero, P.; Witten, E. H.; Reiff, W. M.; Backes, G.; Sanders-Loehr, J.; Jameson, G. B. *J. Am. Chem. Soc.* **1989**, *111*, 9039–9047. (b) Collamati, I.; Dessy, G.; Fares, V. *Inorg. Chim. Acta* **1986**, *111*, 149–155.
(45) Stenkamp, R. E.; Sieker, L. C.; Jensen, L. H. *J. Am. Chem. Soc.* **1984**, *106*, 618–622.

Table IV. Comparison of Structural, Mössbauer, and Magnetic Features of Selected Diiron(III)-Oxo Complexes and Metalloproteins

compd	Fe–O_b,[a] Å	Fe···Fe, Å	Fe–O_b–Fe, deg	Fe–N_{cis},[b] Å	Fe–N_{trans},[b] Å	δ, mm/s	ΔE_Q, mm/s	$-J$,[c] cm^{-1}	ref
2	1.801 (5) 1.793 (4)	3.211 (2)	126.6 (2)	2.116	2.170	0.54	1.81	111	this work
$[Fe_2O(MPDP)(BIPhMe)_2Cl_2]$	1.783 (5) 1.790 (4)	3.183 (2)	125.9 (2)	2.119	2.159	0.52	1.94	122	3b
$[Fe_2O(MPDP)(4,4'\text{-}Me_2bpy)_2Cl_2]$	1.771 (3) 1.774 (3)	3.130 (1)	124.0 (2)	2.155	2.200	0.51	1.66	119	3b
$[Fe_2O(O_2CH)_2(HB(pz)_3)_2]$	1.777 (3) 1.785 (3)	3.1677 (9)	125.5 (2)	2.143	2.179				4a
$[Fe_2O(O_2CCH_3)_2(Me_3TACN)_2]^{2+}$	1.800 (3)	3.12 (4)	119.7 (1)	2.198	2.268	0.47	1.50	119	4c
$[Fe_2O(O_2CCH_3)_2(N3)_2]^{2+}$ [d]	1.777 (5) 1.802 (6)	3.079 (2)	118.7 (3)	2.112	2.287			117	4d
metHr	1.68 1.92	3.21	127	2.19	2.31	0.47	1.57	134	45, 47
$metN_3myoHr$	1.77 1.80	3.23	130	2.13	2.24	0.49	1.96		12, 46
RR	1.79	3.22				0.44 0.53	2.45 1.65	108	16, 18–21
MMO	2.01–2.04[e]	3.44				0.50	1.07		60

[a] O_b refers to the bridging oxygen atom. [b] Fe–$N_{cis/trans}$ refers to average lengths of iron–nitrogen bonds located cis or trans, respectively, to the bridging oxygen ligand. [c] From temperature dependent magnetic susceptibility studies. [d] N3 is bis(2-benzimidazolylmethyl)amine. Note that the amine group is trans, and the benzimidazole groups are cis, to the oxo bridge in this compound. [e] Fe–O/N.

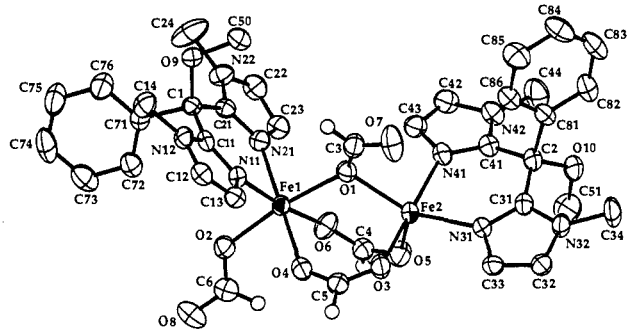

Figure 1. Structure of $[Fe_2(O_2CH)_4(BIPhMe)_2]$ (**1**), showing 60% probability thermal ellipsoids and the atom-labeling scheme. BIPhMe hydrogen atoms are omitted for clarity.

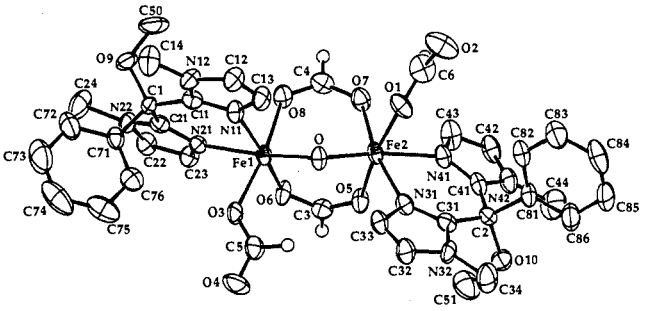

Figure 2. Structure of $[Fe_2O(O_2CH)_4(BIPhMe)_2]$ (**2**), showing 55% probability thermal ellipsoids and the atom-labeling scheme. BIPhMe hydrogen atoms are omitted for clarity.

properties and dioxygen reactivity of **1** with those of reduced RR, is further elaborated in ref 39.

$[Fe_2O(O_2CH)_4(BIPhMe)_2]\cdot 2CH_3OH\cdot H_2O$ ($2\cdot 2CH_3OH\cdot H_2O$). All ligands present in **1** are retained in its oxidation product **2**, which also contains an oxo bridge between the two ferric ions (Figure 2). Capping the well-precedented[1,2] (μ-oxo)bis(μ-carboxylato)diiron(III) core of **2** are two bidentate BIPhMe and two monodentate stereochemically distinct formate ligands, the latter occupying coordination sites cis to the oxo bridge. Each terminal formate is attached to iron via an anti lone pair, a unique situation among ferric carboxylate compounds,[42] and is hydrogen bonded via its second oxygen atom to either a methanol (O2) or a water (O4) solvent molecule in the crystal lattice. A hydrogen-bonded array of water and methanol molecules thus connects individual diiron complexes in adjacent unit cells via the inequivalent terminal carboxylates (see Figure S1, supplementary material for a packing diagram).

The bond lengths and angles of the triply bridging core in **2** are generally similar to those of other structurally characterized (μ-oxo)bis(μ-carboxylato)diiron(III) complexes (Table IV).[2-5,36] Both the Fe···Fe distance of 3.211 (2) Å and the Fe–O_b–Fe angle of 126.6° are larger than in any known diiron(III) complex, however, and most closely approach the values found for metHr and metazidomyoHr (3.21–3.23 Å and 127–130°).[45,46] The only oxo-bridged compounds with more expanded cores either contain a single supporting carboxylate[5] or have additional bridging phosphate or phosphinate ligands instead of carboxylate ligands.[7] Tighter binding of imidazole compared to pyridine, pyrazole, or amine groups to iron may be responsible for the larger intermetal distance and Fe–O–Fe angle in **2** relative to other complexes (Table IV).

As observed for previous model compounds,[2] the Fe–N bond trans to the oxo bridge in **2** is longer than its counterpart in the cis position as a result of the powerful trans influence of the short Fe–(μ-oxo) bond.[4a] In addition, and in agreement with results for $metN_3myoHr$[46] and species having N_2Cl capping donor sets,[3] the Fe–O_{COO} (COO = carboxylate) bond trans to the monodentate terminal ligand is also lengthened. Overall, the structural features of **2** are quite similar to those of $[Fe_2O(MPDP)(BIPhMe)_2Cl_2]$ (MPDP = *m*-phenylenedipropionate), the only other diiron(III)–BIPhMe complex prepared to date.[3b]

$[Zn(BIPhMe)Cl_2]$ (6). Complex **6** contains two imidazoles from a BIPhMe molecule and two chloride ligands bound in a pseudotetrahedral array to a zinc(II) ion (Figure 3). The Zn–N and Zn–Cl bond lengths (Zn–N11 = 2.011 (3) Å, Zn–N21 = 2.002 (3) Å, Zn–Cl1 = 2.243 (1) Å, and Zn–Cl2 = 2.205 (1) Å are unexceptional. Deviation from regular tetrahedral geometry is indicated by the large Cl1–Zn–Cl2 and correspondingly small N11–Zn–N21 angles of 115.98 (4)° and 90.4 (1)°, respectively. The preferred bite angle of the bidentate BIPhMe (ca. 80–85°) and interligand repulsions between the chlorides presumably are responsible for the observed distortion. Similar bond lengths and angles were reported for an analogous compound, $[ZnLBr_2]$ (L = bis(4,5-diisopropyl-1-methyl-2-imidazolyl)ketone).[48] Full tables of bond lengths and angles as well as pertinent crystallographic

(46) Sheriff, S.; Hendrickson, W. A.; Smith, J. L. *J. Mol. Biol.* **1987**, *197*, 273–296.

(47) (a) Okamura, M. Y.; Klotz, I. M.; Johnson, C. E.; Winter, M. R. C.; Williams, R. J. P. *Biochemistry* **1969**, *8*, 1951–1958. (b) Dawson, J. W.; Gray, H. B.; Hoenig, H. E.; Rossman, G. R.; Schredder, J. M.; Wang, R.-H. *Biochemistry* **1972**, *11*, 461–465.

(48) Read, R. J.; James, M. N. G. *Acta Crystallogr.* **1980**, *B36*, 3100–3102.

Table V. Electronic Spectral Features of Selected (μ-Oxo)diiron(III) Model Compounds and Proteins

assignment[a]	**2**	$[Fe_2O(MPDP)(BIPhMe)_2Cl_2]$	$[Fe_2O(O_2CH)_2(HB(pz)_3)_2]$	$metN_3Hr$	RR
LMCT	329 (3400)	341 (4600)	342 (5110)	326 (3375)	325 (4700)
LMCT, $O^{2-} \rightarrow$ Fe CT	354 (sh, 2900)	360 (sh)		380 (sh, 2150)	370 (3600)
$^6A_1 \rightarrow [^4T_2]({}^4D)$	448 (370)		460 (535)	446[b]	
$^6A_1 \rightarrow [^4A_1,{}^4E]({}^4G)$	478 (sh, 340)	483 (400)	489 (480)		500 (400 br)
$O^{2-} \rightarrow$ Fe CT	520 (sh)	525 (sh)	530 (sh)	530 (sh)	
$^6A_1 \rightarrow [^4T_2]({}^4G)$, CT	662 (70)	682 (90)	692 (69)	680 (95)	600 (150)
ref	this work	4b	4a	51a	19, 20

[a] References 49 and 51. [b] Overlapping azide to Fe(III) charge-transfer transition.

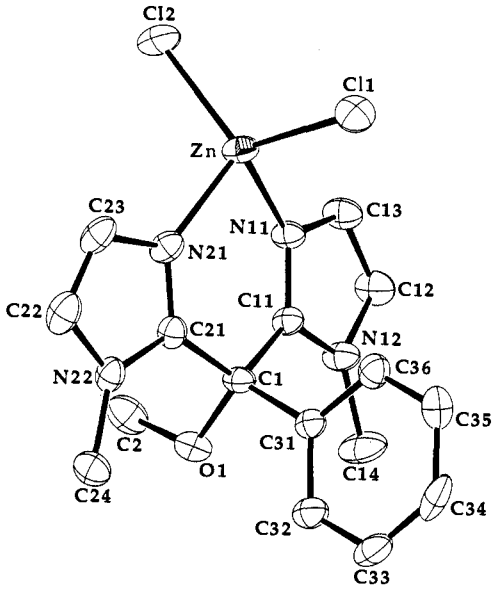

Figure 3. Structure of $[Zn(BIPhMe)Cl_2]$ (**6**), showing 50% probability thermal ellipsoids and the atom-labeling scheme. **BIPh**Me hydrogen atoms are omitted for clarity.

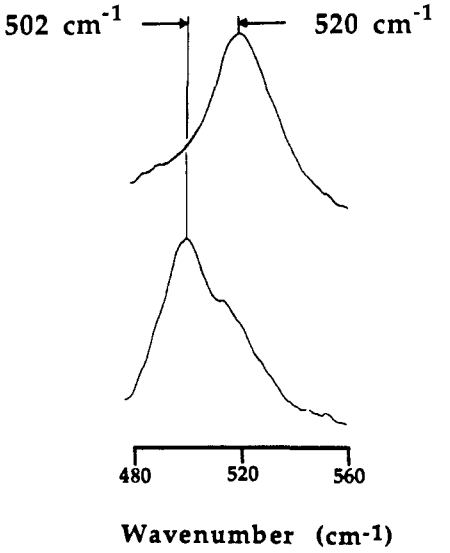

Figure 4. Resonance Raman spectra of $CHCl_3$ solutions of **2** showing ν_s (Fe–O–Fe): (top) ^{16}O-labeled **2** and (bottom) ^{18}O-labeled **2** prepared by exposure of **1** to $^{18}O_2$.

information for **6** are provided as supplementary material.

Electronic and Vibrational Spectroscopy. Optical spectra of solutions of **1** in CH_2Cl_2 or $CHCl_3$ exhibit only a weak (ϵ_M/Fe = 200 cm^{-1} M^{-1}) absorption at 290 nm in the UV–visible region. In contrast, numerous absorption bands characteristic of the (μ-oxo)bis(μ-carboxylato)diiron(III) core are apparent in the spectrum of **2**.[1,2] Absorption maxima and corresponding extinction coefficients for **2**, two other diferric model compounds, $metN_3Hr$ and RR are listed, together with their assignments,[49] for comparison in Table V. Overall, the electronic spectral features among the model compounds and the proteins match quite well. In both BIPhMe complexes **2** and $[Fe_2O(MPDP)(BIPhMe)_2Cl_2]$ the low-energy $^6A_1 \rightarrow [^4T_2]({}^4G)$ ligand field transition occurs at shorter wavelength than in $[Fe_2O(O_2CH)_2(HB(pz)_3)_2]$. These observations underscore the weaker ligand field strength of N_2(imidazole)X versus N_3(pyrazole) terminal donor sets, since ligand field strengths and d–d band energies are inversely correlated for high-spin iron(III).[50] The same sensitivity of this electronic transition to the nature of X in metXHr has been described previously.[51a] The absorption maxima for **2** occur at slightly higher energy than for $[Fe_2O(MPDP)(BIPhMe)_2Cl_2]$, however, which differs in its coordination sphere only as a result of the presence of chloride instead of formate. The difference between alkyl carboxylates and formate is expected to have a negligible effect on the spectral energies.[4a] The implication is that terminal formate is a slightly weaker field ligand compared to chloride, an unexpected result considering the relative positions of chloride and carboxylate in the spectrochemical series ($RCO_2^- > Cl^-$).[50] Possibly the band has some charge-transfer character,[51b] which could account for this result. Finally, we note that the $^6A_1 \rightarrow [^4T_2]({}^4G)$ ligand field transition in RR is shifted to very high energy, consistent with the presence of only two relatively strong field imidazole and a total of six weaker field oxygen donor ligands (two waters and four carboxylates) bound to its diiron(III) site.[22] Compound **2** models the active site of RR inasmuch as its carboxylate-rich core induces analogous, albeit less dramatic, shifts in its electronic absorption spectral features.

The (μ-oxo)diiron(III) unit of **2** also gives rise to distinctive features in its resonance Raman and infrared spectra. The symmetric Fe–O–Fe stretch, ν_s, is located at 520 cm^{-1} in the resonance Raman spectrum (406.7-nm excitation wavelength; Figure 4) on the basis of its shift to 502 cm^{-1} upon ^{18}O substitution by $H_2{}^{18}O$ exchange. Alternatively, isotopically labeled **2** could be prepared by treatment of **1** with $^{18}O_2$ (lower spectrum, Figure 4). These results prove that the oxo bridge in **2** is derived from molecular oxygen and not from adventitious H_2O. The Fe–O–Fe asymmetric stretch, ν_{as}, is obscured by ligand absorptions in the FTIR spectrum of **2** but was located by subtraction from the spectrum of the ^{18}O-labeled complex (ν_{as} (^{16}O) = 760 cm^{-1}; ν_{as} (^{18}O) = 708 cm^{-1}, data not shown). A weak feature in the FTIR spectrum at 518 cm^{-1}, that shifts to 500 cm^{-1} upon ^{18}O substitution, may be the symmetric vibration, since the values match those in the resonance Raman spectrum. By using the measured values of ν_s and ν_{as} and equations previously derived for structures with local C_{2v} symmetry,[52] the stretch (k_d) and stretch–stretch interaction (k_{dd}) force constants were calculated to be 3.21 and 0.49 mdyne/Å, re-

(49) Schugar, H. J.; Rossman, G. R.; Barraclough, C. G.; Gray, H. B. *J. Am. Chem. Soc.* **1972**, *94*, 2683–2690.
(50) Figgis, B. N. *Introduction to Ligand Fields*; John Wiley & Sons: New York, 1966.
(51) (a) Reem, R. C.; McCormick, J. M.; Richardson, D. E.; Devlin, F. J.; Stephens, P. J.; Musselman, R. L.; Solomon, E. I. *J. Am. Chem. Soc.* **1989**, *111*, 4688–4704. (b) Butcher, K. D.; Gebhard, M. S.; Solomon, E. I. *Inorg. Chem.* **1990**, *29*, 2067–2074.
(52) (a) Wing, R. M.; Callahan, K. P. *Inorg. Chem.* **1969**, *8*, 871–874. (b) Cotton, F. A.; Wing, R. M. *Ibid.* **1965**, *4*, 867–873. (c) Nakamoto, K. *Infrared and Raman Spectra of Inorganic and Coordination Compounds*, 4th ed.; John Wiley & Sons: New York, 1986; pp 59–62.

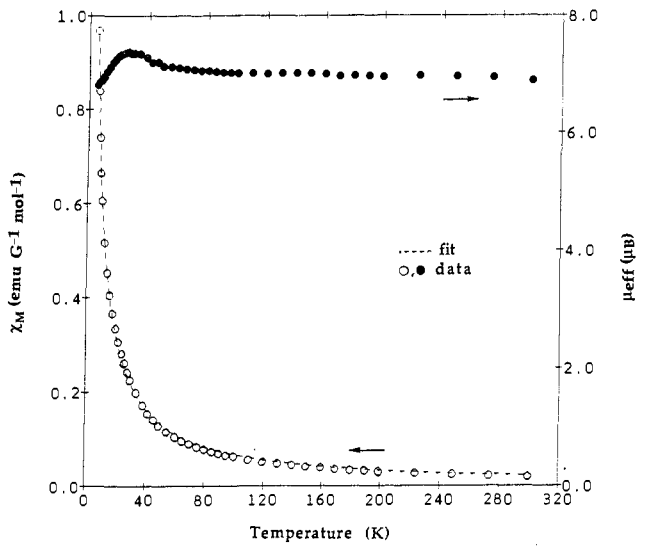

Figure 5. Plot of χ_M (O; emu G^{-1} mol^{-1}) and μ_{eff} (●; μ_B) versus temperature (K) for solid **1**. The dashed line represents a least-squares fit to the data as described in the text.

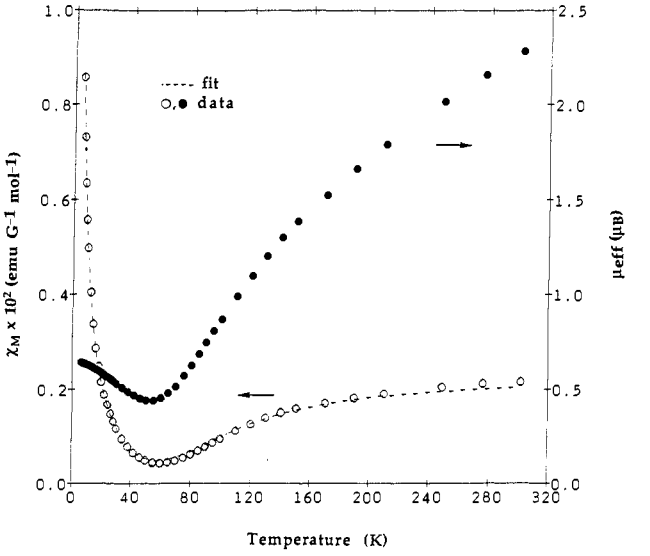

Figure 6. Plot of χ_M (O; emu G^{-1} mol^{-1}) and μ_{eff} (●; μ_B) versus temperature (K) for solid **2**·H_2O. The dashed line represents a least-squares fit to the data as described in the text.

spectively. Similar values have been reported for other (μ-oxo)bis(μ-carboxylato)diiron(III) complexes.[2,4a,7c,53] These force constants predict respective frequencies for the symmetric and asymmetric vibrations for the ^{18}O derivative of 503 and 702 cm^{-1}, in good agreement with the experimentally determined numbers (502 and 708 cm^{-1}). Finally, the Fe–O–Fe angle can be calculated from ν_s by using an empirical expression that relates the cosine of the angle with the square of the Fe–O–Fe vibrational frequency.[7c] The resulting value of 123° agrees satisfactorily with the angle determined by X-ray crystallography (126.6°).

Magnetic Susceptibility Measurements. Solid-state magnetic susceptibility data for **1** and **2**·H_2O are shown in Figures 5 and 6 as plots of χ (emu G^{-1} mol^{-1}) and μ_{eff} (μ_B) per dinuclear complex versus temperature. Inspection of the data for **1** in Figure 5 reveals little or no exchange coupling between the two ferrous centers in the complex. This conclusion is supported by various approximate fits to the data, none of which explicitly accounted for spin-orbit coupling or zero-field splitting. The least-squares fit shown as a dashed line in Figure 5 was calculated by using an expression derived from the general isotropic Hamiltonian $\mathcal{H} = -2JS_1 \cdot S_2$,

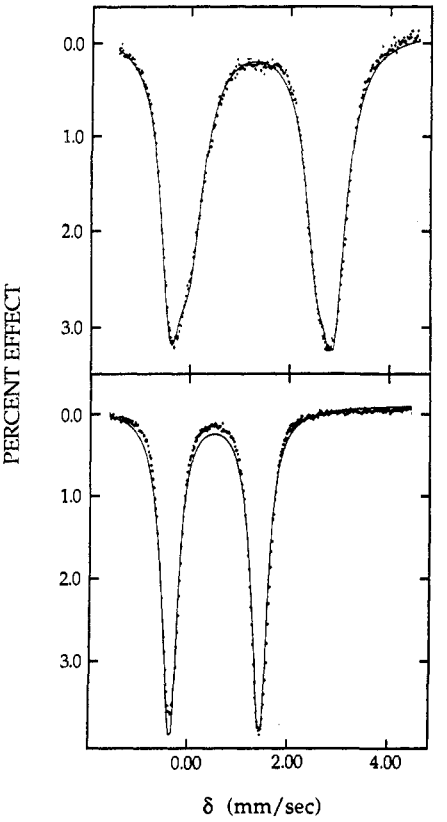

Figure 7. Zero-field Mössbauer spectra of polycrystalline samples of **1** (top) and **2**·H_2O (bottom) at 4.2 K. The solid lines are least-squares fits to the data as described in the text.

where $S_1 = S_2 = 2$.[4c,33] Varying J and g gave $J = -0.16$ (1) cm^{-1} and $g = 2.122$ (7) with a correlation coefficient (R) of 0.9997. An alternative fit using the Curie–Weiss expression yielded $C = 3.41$ (2) and $\theta = -1.1$ (6) K with $R = 0.9997$. The calculated C corresponds to a g value of 2.13 (1) that is similar to parameters determined for other diiron(II) complexes.[54] Because complicated energy level distributions arise when $|J| \sim |D|$ (D = zero-field splitting parameter),[10b] the small magnitude of J calculated above suggests that exclusion of D from the fit is unjustified and that the calculated fit is probably not unique. Nevertheless, the data clearly indicate the absence of significant magnetic exchange coupling in **1**, in contrast to results for deoxyHr ($J = -13$ to -26 cm^{-1})[10,11] and the hydroxo-bridged complex **3** ($J = -13$ cm^{-1}).[4c] Assuming that the dominant magnetic exchange pathway is through the bridging oxygen atom in both **1** and **3**, the significantly longer bond distances to that atom in **1** may explain the weakness of its exchange interaction.

The best least-squares fit to the data for **2**·H_2O (dashed line, Figure 6) gave $J = -110.8$ (6) cm^{-1}, PIP ($S = {}^5/_2$ impurity) = 1.255 (4)%, TIP = −6.7 (1) × 10^{-4}, and $R = 0.9998$. The magnitude of the antiferromagnetic exchange constant for **2** is similar to those reported for other (μ-oxo)bis(μ-carboxylato)diiron(III) complexes[2,4] and is almost identical with the value determined for $[Fe_2O(O_2CCH_3)_2\{[OP(OEt)_2]_3Co(C_5H_5)\}_2]$ (108.5 (4) cm^{-1}),[4g] a complex with a similar Fe–(μ-O) distance (1.795 vs 1.797 Å for **2**). Insertion of the value for **2** into an empirical equation relating such distances with J in diiron(III) compounds with two or more bridging ligands[7c,55] yields a coupling constant of −115 cm^{-1}, in satisfactory agreement with the experimentally determined result (−111 cm^{-1}).

Mössbauer Spectroscopy. Zero-field Mössbauer spectra of polycrystalline samples of **1** and **2**·H_2O were obtained at 4.2–230

(53) Spool, A.; Williams, I. D.; Lippard, S. J. *Inorg. Chem.* **1985**, *24*, 2156–2162.

(54) (a) Lambert, S. L.; Hendrickson, D. N. *Inorg. Chem.* **1979**, *18*, 2683–2686. (b) Spiro, C. L.; Lambert, S. L.; Smith, T. J.; Duesler, E. N.; Gagne, R. R.; Hendrickson, D. N. *Ibid.* **1981**, *20*, 1229–1237.

(55) Gorun, S. M.; Lippard, S. J. *Recl. Trav. Chim. Pays-Bas* **1987**, *106*, 417.

and 4.2–80 K, respectively. Representative spectra and theoretical least-squares fits to the data are shown in Figure 7. The Mössbauer spectrum of **1** at 4.2 K consists of two overlapping quadrupole doublets, as revealed by the breadth and asymmetry of the exhibited signal. The best fit to the data (Figure 7, top) indicates the presence of inequivalent ferrous centers in the complex with similar isomer shifts (δ) but significantly different quadrupole splitting parameters (ΔE_Q; Table III). The intensity and quadrupole splittings at each site vary independently with temperature (data not shown), further supporting the inequivalence of the coordination environments of the iron atoms and suggesting the presence of low-lying excited states. We ascribe the larger ΔE_Q value to the inherently more asymmetric pentacoordinate iron atom. This assignment is supported by the similarly disparate values found for **5** (Table III),[35] in which a 2:1 ratio of doublets corresponds to the ratio of five- and six-coordinate ferrous ions present in the complex. A larger ΔE_Q value is observed for the pentacoordinate sites in **5** compared to that for **1**, presumably because the iron atoms in the former more closely approach the less symmetric (relative to octahedral) trigonal-bipyramidal geometry.[35]

The Mössbauer spectral parameters for **1** are compared to those of the other diiron(II) complexes **3** and **4** and to the reduced forms of the proteins Hr, RR, and MMO in Table III. All exhibit isomer shifts and quadrupole splittings typical for high-spin iron(II) in O,N donor ligand environments. Surprisingly, despite the spectroscopic[10,11] and X-ray structural evidence[8] in favor of an asymmetric structure for deoxyHr, only one quadrupole doublet is observed in its Mössbauer spectrum.[12] This discrepancy can be explained either by postulating that the prevailing structural model for the active site of deoxyHr is incorrect or that the available Mössbauer data cannot distinguish between the five- and six-coordinate metal centers. The observation of distinct quadrupole doublets for **1** and, at low temperatures, for the even more symmetric **4**[26] suggests that the different sites in deoxyHr ought to be discernable by Mössbauer spectroscopy. More detailed studies of the physical properties of the protein and of other bridged diiron(II) complexes are clearly warranted. Finally, the Mössbauer parameters for the reduced forms of RR and MMO are similar to those exhibited by the pentacoordinate iron of **1**, suggesting the presence of rather asymmetric ligand environments in these systems.

The Mössbauer spectrum of **2** (Figure 7, bottom) consists of a single quadrupole doublet with an isomer shift typical for high-spin iron(III) and a large ΔE_Q value characteristic of an oxo-bridged complex (Table IV).[1,2] The spectral parameters are unremarkable in comparison to other (μ-oxo)bis(μ-carboxylato)diiron(III) complexes and accurately model the properties of the oxidized forms of Hr. The asymmetric spectrum of RR and the anomalously low ΔE_Q value observed for MMO differ significantly from the Mössbauer features of **2** and the other diiron(III) model compounds, however, supporting the known[22] or purported[23,25] differences in the structures of the active sites of these proteins compared to Hr.

^{1}H NMR Spectroscopy. The 250-MHz ^{1}H-NMR spectrum of a solution of **1** in CD_2Cl_2 at 297 K is presented in Figure 8 (top). With the exception of a broad resonance at ca. −3 ppm (not displayed), no peaks other than the ones shown were observed between +300 and −180 ppm. The absence of signals downfield of 50 ppm is in marked contrast to the spectrum reported for **4**, which contains several assignable resonances between 50 and 200 ppm.[26b] The peaks exhibited in the spectrum of **1** generally have relatively narrow line widths consistent with short electron spin–lattice relaxation times (T_1's) normally associated with high-spin Fe(II).[56] The number of observed signals is fewer than expected on the basis of the asymmetric structure of **1** determined in the solid state (28 peaks total), however, suggesting either fortuitous overlapping of resonances or fluxional behavior resulting in peak averaging.

The peak assignments shown in Figure 8 were deduced from deuterium substitution, T_1 measurements, and consideration of relative isotropic shifts (Table VI). Isotropic shifts ($\Delta H/H^{iso}$)

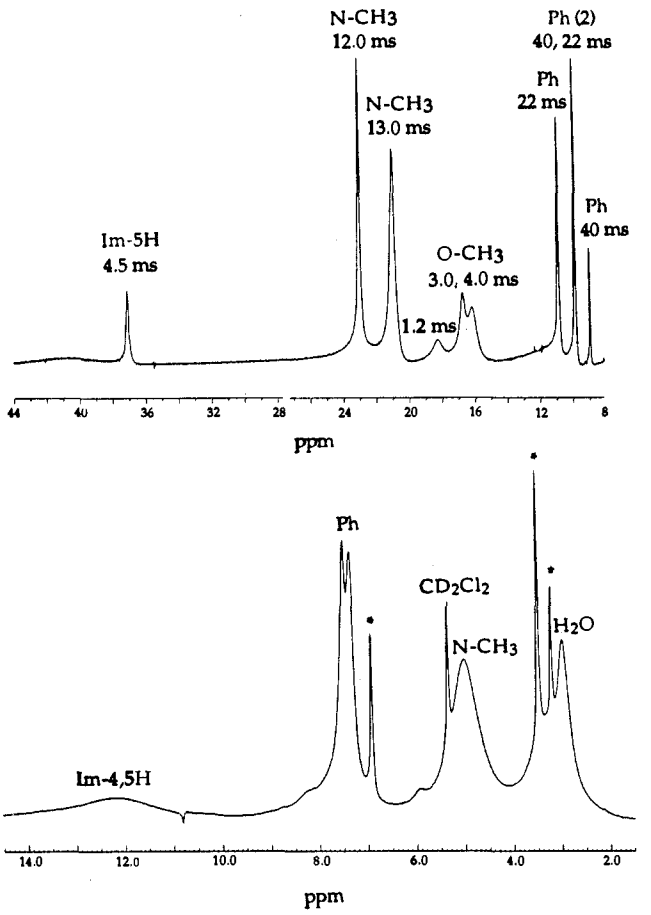

Figure 8. ^{1}H-NMR spectra and proposed assignments of solutions of **1** in CD_2Cl_2 (top; with T_1 values) and **2**·H_2O in a mixture of CD_2Cl_2 and CD_3OD (bottom; * = dissociated BIPhMe) at 297 K.

for the coordinated BIPhMe ligands, which can have both contact and dipolar contributions,[56] were obtained by subtracting the chemical shifts measured for the diamagnetic reference compound **6** from the appropriate resonances in the spectrum of **1**. Simple replacement of the *N*-methyl and/or *O*-methyl groups of the BIPhMe ligand with deuteriomethyl substituents allowed unequivocal identification of their respective resonances. The sharp peaks at ~10 ppm were assigned on the basis of their small isotropic shifts and large T_1 values (Table VI) to hydrogens on the phenyl ring of BIPhMe, which are relatively far (>6 Å) from the iron centers. Conversely, the large $\Delta H/H^{iso}$ and short T_1 value for the resonance at 37 ppm indicates that it arises from hydrogens in close proximity to a Fe(II) center. We tentatively ascribe this signal to the imidazole ring H5-protons, which lie ~5 Å from the closest metal center. Resonances due to the formate hydrogen atoms were not located, the ^{1}H NMR spectrum of **1** prepared from $Fe(O_2CD)_2 \cdot 2H_2O$ being indistinguishable from that exhibited in Figure 8. Presumably, these resonances are broadened into the baseline. We so far have been unable to assign the peaks at ~41 (br), 22.5 (br, only observed in the spectrum of **1** with fully deuterated methyl groups), 18, 12 (br), and −3 ppm (br).

Several pieces of evidence support the occurrence of significant dipolar contributions to the isotropic shifts of **1**. Comparison to the ^{1}H NMR spectra of $[(N\text{-RIm})_6Fe](X)_2$ (RIm = 1-alkylimidazolyl; R = Me or Et; X = BF_4 or BPh_4) is informative, since the isotropic shifts reported for these compounds (Table VI) have been suggested to be purely contact shifted resonances.[4h] The

(56) (a) Bertini, I.; Luchinat, C. *NMR of Paramagnetic Molecules in Biological Systems*; Benjamin/Cummings: Menlo Park, CA, 1986. (b) Horrocks, W. deW., Jr. In *NMR of Paramagnetic Molecules*; La Mar, G. N., Horrocks, W. deW., Jr., Holm, R. H., Eds.; Academic Press: New York, 1973; pp 127–177. (c) La Mar, G. N. *Ibid.* pp 85–126. (d) Que, L., Jr.; Lauffer, R. B.; Lynch, J. B.; Murch, B. P.; Pyrz, J. W. *J. Am. Chem. Soc.* **1987**, *109*, 5381–5385.

Table VI. ^{1}H-NMR data for **1**,**2**·H_2O, and $[Fe(N\text{-Etlm})_6]^{2+}$ [4h]

assignment	1[a]	$[Fe(N\text{-FeIm})_6]^{2+}$ [a]	**2**·H_2O[b]
N–C*H*	19.5 (12), 17.3 (13)	4.6 (66)	5.0
imidazole-5*H*	29.5 (4.5)[c]	39.5 (40)	12.3
imidazole-4*H*		24.7 (2.8)	12.3
imidazole-2*H*		15.6 (2.7)	
O–C*H*	14.0 (3), 12.6 (4)		~3
Ph	3.3 (22), 2.4 (22), 2.4 (40), 1.5 (40)		7.3, 7.4

[a] Data reported as isotropic shifts (T_1 value) in units of ppm (ms). For **1**, isotropic shifts were calculated by subtracting the chemical shifts of **6** from those observed for **1**. For $[Fe(N\text{-Etlm})_6]^{2+}$, isotropic shifts were calculated from the published chemical shifts[4h] by subtracting of the data for **6** (the diamagnetic shift for the imidazole-2*H* proton was estimated to be 7.5 ppm). [b] Data reported as chemical shifts in units of ppm. [c] Tentative assignment, see text.

absence of dipolar contributions to their shifts is expected on the basis of the octahedral symmetry[4h,56] and was confirmed by the Curie temperature dependencies of their shifts above 250 K.[4h] The isotropic shifts of the *N*-methyl resonances for **1** are significantly greater than for $[(N\text{-MeIm})_6Fe](BPh_4)_2$ ($\Delta\Delta H/H^{iso} \sim 13$ ppm), arguing for the presence of dipolar contributions in **1**. In addition, the T_1 values for the *N*-methyl hydrogens in **1** are significantly less ($\Delta T_1 \sim 52$ ms) than in the mononuclear complexes. Moreover, in **1** large isotropic shifts and very short T_1 values are observed for the *O*-methyl hydrogen atoms, which are six bonds removed from the Fe(II) centers yet lie approximately 5 Å away. The correspondence between the *O*-methyl and imidazole 5-hydrogen T_1 values and Fe···H distances (~5 Å) and the unlikelihood of there being appreciable through-bond interactions with the ferrous ion electrons are consistent with significant dipolar (through-space) effects.

Variable-temperature ^{1}H-NMR spectra of **1** were measured in order to assess further the relative importance of the contact and dipolar influences as well as to uncover any fluxional behavior. The results (Figures S2 and S3, supplementary material) were ambiguous, however. Plots of the isotropic shifts versus T^{-1} for some peaks (imidazole 5-H, one *N*-methyl, and the sharp phenyl resonances) gave straight lines as predicted by the Curie law, whereas other signals showed more complicated behavior, including non-Curie deviations from linearity in $\Delta H/H^{iso}$ vs T^{-1} plots, splitting into separate peaks at lower temperatures, and exhibiting unresolvable broadening. These results and the reversibility of the spectral changes upon raising or lowering the temperature argue for dipolar influences and/or fluxionality and against sample decomposition. We have been unable to differentiate between the former possibilities and must therefore conclude that, in solution, intra- or intermolecular ligand exchange phenomena may be important.

The ^{1}H-NMR spectrum of a solution of **2**·H_2O in a mixture of CD_2Cl_2 and CD_3OD (to enhance solubility) at ~300 K is shown in Figure 8 (bottom). As with other (μ-oxo)bis(μ-carboxylato)diiron(III) compounds, **2** exhibits small isotropic shifts owing to strong antiferromagnetic exchange coupling that affords a diminished room temperature effective magnetic moment for the complex (~2.3 μ_B). The appearance of resonances due to the free BIPhMe ligand indicates a small amount of decomposition of the complex in solution. The assignments of the remaining peaks were made by comparison to spectra of *N*-methyl and/or *O*-methyl deuterated derivatives of **2** and to other imidazole-containing oxo-bridged diiron(III) complexes (Table VI).[3b,4h,57] In contrast to $[Fe_2O(O_2CCH_3)_2(TMIP)_2]^{2+}$ (TMIP = tris(1-methylimidazolyl)phosphine), which exhibits two separate imidazole 5-H resonances corresponding to rings cis or trans to the oxo bridge,[4h] only one broad peak at 12.3 ppm assignable to the imidazole hydrogens is apparent in the spectrum of **2**. A single such peak was also observed in this region in the spectra of $[Fe_2O(MPDP)(L)_2Cl_2]$ (L = BIPhMe or TMICMe, tris(1-methylimidazolyl)methoxymethane).[57] The signals at ~7.4 ppm are attributed to the BIPhMe phenyl hydrogens, which are expected to exhibit negligible isotropic shifts because of the large number of intervening bonds to the metal atoms; dipolar terms are insignificant for high-spin Fe(III).[56] The intense, broad resonance at 5.0 ppm disappears upon *N*-methyl deuteration and is thus unequivocally assigned. Comparison to the spectra of $[Fe_2O(MPDP)(L)_2Cl_2]$ complexes indicates that the *O*-methyl peak should appear at ~3 ppm,[57] and thus is probably buried under the H_2O and dissociated BIPhMe peaks. Finally, as previously noted for $[Fe_2O(O_2CH)_2(HB(pz)_3)_2]$,[4a] the formate hydrogens in **2** are apparently broadened into the baseline and are unobserved.

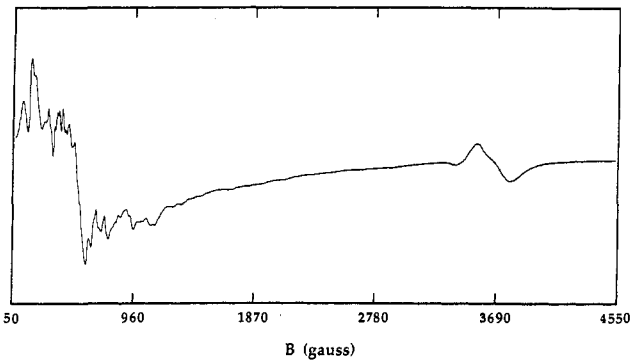

Figure 9. EPR spectrum of a frozen solution of **1** in CH_2Cl_2 at 4 K. Conditions: frequency, 9.42 GHz; power, 20 mW; modulation frequency, 100 KHz; modulation amplitude, 7.86; gain, 1×10^5; sweep time, 168 s.

EPR Spectroscopy. The X-band EPR spectrum of a frozen solution of **1** in CH_2Cl_2 at 4 K is shown in Figure 9. Two features are visible, one at $g \sim 16$ which we assign to an integer spin resonance analogous to those observed for other Fe(II)-containing complexes and proteins,[26b,58] and the other at $g \sim 1.9$. The presence of hyperfine interactions in the former signal is suggested by its unusual line shape at 4 K. While these sharp features remained unchanged as the microwave power was varied at 4 K, they were reversibly lost upon warming of the sample to ~14 K, resulting in a broad resonance more similar to the low field signals reported for other diferrous systems. So far, our preliminary investigation of the $g \sim 16$ resonance of **1** has failed to reveal the basis for its unique appearance.

Integration of the higher field resonance (Figure 9) revealed that it arose from less than 1% of the iron species present in the sample. Treatment of solutions of **1** with air (vide infra) increased the signal to an intensity corresponding to ~5% of the sample, suggesting that the feature is due to an impurity formed by air oxidation of **1**. Similarities between the *g* values and line shapes of this resonance and those reported for Fe(II)Fe(III) forms of Hr[59] and MMO[25,60] support a mixed-valent formulation for the impurity. To allow further comparisons to the mixed-valent forms of the diiron proteins, and with the hope of shedding light on the nature of the bridging ligands of this species, power saturation measurements of the $g \sim 1.9$ signal were carried out. Such experiments allow the antiferromagnetic exchange coupling constant between the iron atoms to be estimated and have been successfully applied to various forms of semimetHr and to the mixed-valent form of MMO.[59,60]

Initial explorations of the dependence of the line shape of the $g \sim 1.9$ signal with increasing microwave power (20 nW–20 mW)

(57) Beer, R. H. Ph.D. Thesis, Massachusetts Institute of Technology, 1990.

(58) (a) Hendrich, M. P.; Debrunner, P. G. *Biophys. J.* **1989**, *56*, 489–506. (b) Hendrich, M. P.; Münck, E.; Fox, B. G.; Lipscomb, J. D. *J. Am. Chem. Soc.* **1990**, *112*, 5861–5865.

(59) (a) Nocek, J. M.; Kurtz, D. M., Jr.; Sage, J. T.; Xia, Y.-M.; Debrunner, P.; Shiemke, A. K.; Sanders-Loehr, J.; Loehr, T. M. *Biochemistry* **1988**, *27*, 1014–1024. (b) Pearce, L. L.; Kurtz, D. M., Jr.; Xia, Y.-M.; Debrunner, P. G. *J. Am. Chem. Soc.* **1987**, *109*, 7286–7293.

(60) DeWitt, J. G.; Bentsen, J. G.; Rosenzweig, A. C.; Hedman, B.; Green, J.; Pilkington, S.; Papaefthymiou, G. C.; Dalton, H.; Hodgson, K. O.; Lippard, S. J. To be submitted for publication.

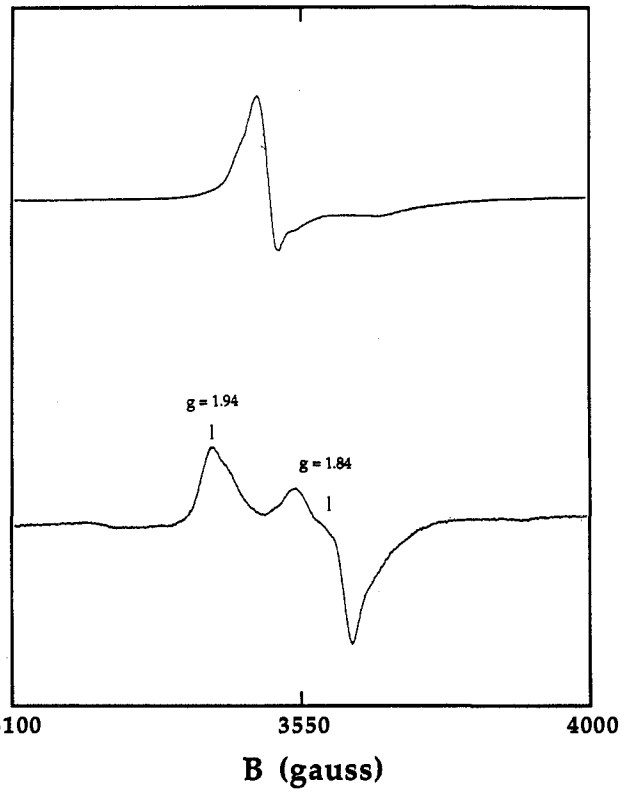

Figure 10. EPR spectrum at 4 K of frozen solution of **1** in CH_2Cl_2 briefly exposed to air at −78 °C (top) or at room temperature (bottom). Power saturation data were collected for the lower signal. Conditions were the same as reported in Figure 9, except for the power (2 mW) and modulation amplitude (16).

and/or temperature (6–20 K) indicated that the species present depended on the method of air oxidation of **1**. Bubbling of dry air through a solution of **1** in CH_2Cl_2 at −78 °C resulted in a resonance (Figure 10, top) that clearly was derived from a mixture of species, since drastic changes in line shape occurred as the microwave power or temperature was varied. Brief (<30 s) air oxidation of a solution of **1** at room temperature followed immediately by rapid freezing resulted in a different signal (Figure 10, bottom), the line shape of which was independent of microwave power. This resonance proved to be amenable to power saturation measurements[34] and thus to the estimation of the antiferromagnetic exchange interaction between the iron atoms in the mixed-valent species.

Values of the half saturation power ($P_{1/2}$) were determined graphically and plotted on a log scale versus the inverse of the temperature according to previously described methods (Figure 11).[34,59,60] Linear behavior is consistent with predominant spin relaxation by the Orbach mechanism. The five highest temperature points were fit to a straight line (R = 0.995) of slope Δ/k = −134 (7), where $\Delta \sim 3J$ and k is the Boltzmann constant. Deviation from the line at the lowest temperature point indicates the onset of direct relaxation processes.[34] The resulting J value of −31 (2) cm^{-1} is identical with that found for the mixed-valent form of protein A of MMO[60] and is slightly larger than those determined for various semimetHr samples (J = −15 to −29 cm^{-1}, the latter value being for the sulfide bridged analogue).[59] Although structural information for the species responsible for the $g \sim 1.9$ signal formed upon oxidation of **1** is not currently available, reasonable candidates for the bridge between the Fe(II) and Fe(III) atoms that gives rise to the observed antiferromagnetic exchange coupling are oxo, a monodentate formate, or possibly a monodentate superoxo ligand.

Mechanism of the Conversion of 1 to 2. Although the nearly quantitative formation of an oxo-bridged diiron(III) center as a result of aerial oxidation of a diiron(II) complex is rare,[4b,c] the conversion of **1** to **2** has parallels in the dioxygen reactivity of

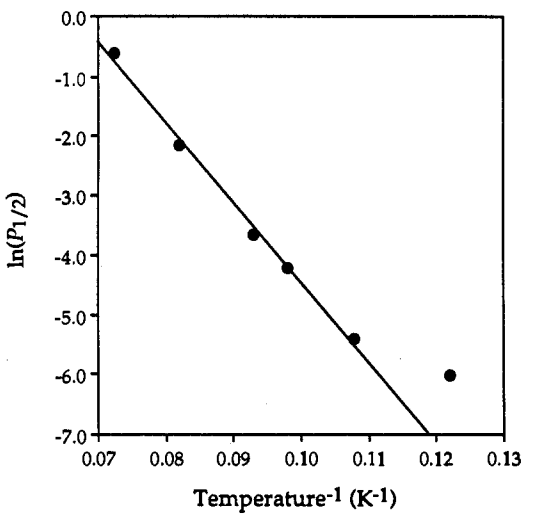

Figure 11. Plot of ln ($P_{1/2}$) versus temperature^{-1} (K^{-1}) for the EPR signal obtained upon brief exposure of a solution of **1** in CH_2Cl_2 to air at room temperature.

mononuclear ferrous complexes.[61-63] For example, the conversion of ferrous porphyrins (PFe^{II}) to oxo-bridged dinuclear complexes $[PFe^{III}]_2O$ upon exposure to molecular oxygen is a well-known transformation[62,63] that had to be circumvented before the reversible binding of dioxygen to hemoglobin could be modeled in synthetic systems.[62,64] The accepted mechanism for the formation of $[PFe^{III}]_2O$ from PFe^{II} involves initial binding of O_2 followed by dimerization with another molecule of PFe^{II} to give a peroxo-bridged diferric species (eq 4). Subsequent cleavage of the

$$PFe^{II} \xrightarrow{O_2} PFe^{III}O_2 \xrightarrow{PFe^{II}} PFe^{III}OOFe^{III}P \rightarrow PFe^{IV}O \xrightarrow{PFe^{II}} PFe^{III}OFe^{III}P \quad (4)$$

peroxo-bridged dimer is believed to provide highly reactive Fe(IV)–oxo monomers that combine with PFe^{II} to afford the isolated (μ-oxo)diiron(III) product. Direct spectroscopic evidence is available for several of the proposed intermediates, including the peroxo-bridged dimer.[63]

An analogous route to that shown in eq 4 can be envisaged for the production of **2** from **1** (Scheme III, pathway A). Binding of O_2 to **1** might yield a mixed-valent $Fe^{III}Fe^{II}$–superoxo complex that could be trapped by a second molecule of **1** to afford a peroxo-bridged tetranuclear $[Fe^{III}_2Fe^{II}_2]$ intermediate. The geometry suggested for the latter compound has precedence in the recent discovery of a stable, structurally characterized Fe^{III}_4–η^2:η^2-peroxo unit within a larger polyiron aggregate.[65] Compound **2** could arise via cleavage of the mixed-valent tetrairon intermediate followed by electron transfer and collapse to (μ-oxo)diiron(III) species. Alternatively, the initial, probably highly reactive, adduct formed by O_2 binding to **1** might react oxidatively with solvent, adventitious protons, or the ligands, thus transferring

(61) For selected non-heme iron cases, see: Murray, K. S. *Coord. Chem. Rev.* **1974**, *12*, 1–35.
(62) Review: Collman, J. P.; Halbert, T. R.; Suslick, K. S. In *Metal Ion Activation of Dioxygen*; Spiro, T. G., Ed.; John Wiley & Sons: New York, 1980; pp 1–72.
(63) See, for example: (a) Chin, D. H.; DelGaudio, J.; LaMar, G. N.; Balch, A. L. *J. Am. Chem. Soc.* **1977**, *99*, 5486. (b) Paeng, I. R.; Shiwaku, H.; Nakamoto, K. *J. Am. Chem. Soc.* **1988**, *110*, 1995–1996, and references cited therein.
(64) (a) Collman, J. P.; Gagne, R. R.; Halbert, T. R.; Marchon, J. C.; Reed, C. A. *J. Am. Chem. Soc.* **1973**, *95*, 7860. (b) Almog, J.; Baldwin, J. E.; Huff, J. *Ibid.* **1975**, *97*, 227. (c) Collman, J. P.; Gagne, R. R.; Reed, C. A.; Halbert, T. R.; Lang, G.; Robinson, W. T. *Ibid.* **1975**, *97*, 1427. (d) Collman, J. P.; Brauman, J. I.; Doxsee, K. M.; Halbert, T. R.; Suslick, K. *Proc. Natl. Acad. Sci. U.S.A.* **1978**, *75*, 564. (e) Dieckmann, D.; Chang, C. K.; Traylor, T. G. *J. Am. Chem. Soc.* **1971**, *93*, 4068.
(65) Micklitz, W.; Bott, S. G.; Bentsen, J. G.; Lippard, S. J. *J. Am. Chem. Soc.* **1989**, *111*, 372–374.

Scheme III

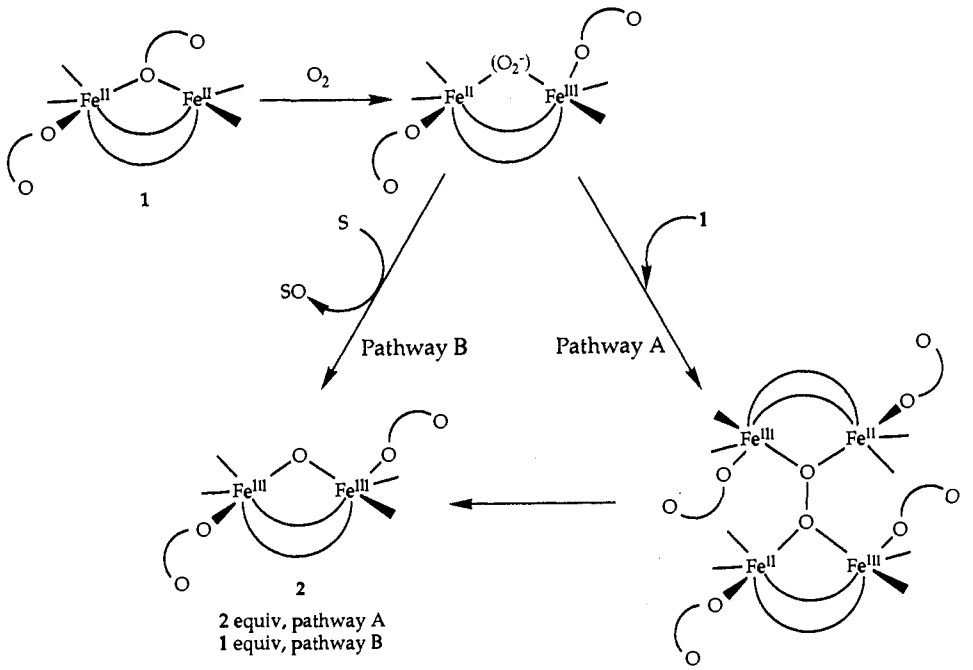

an oxygen atom to substrate and forming **2** directly (Scheme III, pathway B).

Since the two pathways in Scheme III differ with regard to their stoichiometry, route A using 0.5 mol of O_2 per mol of **1** while route B uses 1.0 mol, manometric measurements of dioxygen uptake in the conversion of **1** to **2** were carried out to distinguish between them. The finding that 0.6 (1) mol of O_2 are consumed per mol of **1** argues strongly for a mechanism such as A, in which both oxygen atoms of the O_2 molecule are incorporated into product. The slight deviation of the observed stoichiometry from 0.5:1 O_2/**1** may arise from competing side reactions that consume dioxygen, since monitoring of the system by optical spectroscopy revealed formation of small amounts of uncharacterized materials in addition to **2**. Nonetheless, the high overall yield for the production of **2** argues against significant oxidative consumption of the ligands, a possible source of electrons in mechanism B (Scheme III).

The observation of a magnetically exchange coupled mixed-valent species by EPR spectroscopy in solutions of **1** exposed to dioxygen is consistent with the proposed initial reaction step, formation of a dinuclear $Fe^{III}Fe^{II}$–superoxo complex (Scheme III). Direct binding of dioxygen to **1** to form such a species is unlikely, however. Although the pentacoordinate iron atom in **1** has a potentially available coordination site, the "dangling" oxygen atom of the bridging formate appears to block this position. Preliminry attempts to coordinate other exogenous ligands, including halides, CO, OH^-, NO, and PPh_3, to this site have not been successful,[66] arguing for steric inhibition by the formate oxygen atom. Clearly, some type of rearrangement of carboxylates about the core of **1** must occur upon air oxidation. Cleavage of **1** to mononuclear species is also possible. Future experiments are planned in order to address these issues.

Concluding Remarks. The present investigation has provided a non-heme diiron(II) complex (**1**) of potential relevance to the physical and chemical properties of the reduced forms of polyiron–oxo proteins. From its composition, $[Fe_2(O_2CH)_4(BIPhMe)_2]$, it would have been difficult to anticipate the novel asymmetric structure of **1** in which one iron center is pentacoordinate and the other, six-coordinate. The bridging monodentate formate ligand illustrates a possible mode of carboxylate coordination that, while not yet assigned to the Fourier map electron density in any iron–oxo protein X-ray structural work, must surely be a candidate for the reduced centers in the proteins RR and MMO. Although the dangling oxygen atom in **1** blocks coordination of simple electron pair donor ligands to the pentacoordinate iron atom, O_2 reacts in a nearly quantitative manner to afford the dinuclear complex $[Fe_2O(O_2CH)_4(BIPhMe)_2]$ (**2**). Both atoms of dioxygen are incorporated into the product, but details of the mechanism by which this oxidation reaction occurs remain to be clarified.[67] Aspects of the transformation of **1** to **2** by O_2 are relevant to the functional activity of RR and MMO. In both biomolecules, reduced diiron(II) centers react with dioxygen ultimately to afford (μ-oxo)diiron(III) cores. In apparent contrast to the conversion of **1** to **2**, however, substrate oxidation accompanies oxo bridge formation in the proteins. Thus, in RR a tyrosyl radical is generated, while, in MMO, methane hydroxylation is catalyzed concomitantly. Further model studies are in progress to address these intriguing features of the protein chemistry and to learn how nature manages to tune the properties of the diiron–oxo protein cores to achieve such diverse functional activities.

Acknowledgment. This work was supported by the National Institutes of Health Grant GM-32134 from the National Institutes of General Medical Sciences. W.B.T. and J.G.B. acknowledge the American Cancer Society for postdoctoral fellowships. We thank Professor A. Bino for his help in initiating this project, Dr. G. C. Papaefthymiou for obtaining Mössbauer spectra, Professor L. Que, Jr. for supplying a preprint of ref 26b, and R. H. Beer, X. Feng, P. Poganiuch, R. L. Rardin, E. I. Solomon, and P. N. Turowski for helpful discussions.

Supplementary Material Available: A packing diagram for **2**·$2CH_3OH·H_2O$, variable-temperature ^1H NMR data for **1**, and tables of bond distances and angles, positional parameters and B(eq) values for all atoms, and thermal parameters for all nonhydrogen atoms (34 pages); tables of observed and calculated structure factors for **1**·$CHCl_3·CH_3CN$, **2**·$2CH_3OH·H_2O$, and **6** (107 pages). Ordering information is given on any current masthead page.

(66) Tolman, W. B.; Poganiuch, P.; Taft, K. L.; Lippard, S. J. Unpublished results.

(67) **Note Added in Proof**: Two papers have recently appeared of possible relevance to this chemistry: Kitajima, N.; Fukui, H.; Moro-aka, Y.; Mizutani, Y.; Kitagawa, T. *J. Am. Chem. Soc.* **1990**, *112*, 6402–6403. Menage, S.; Brennan, B. A.; Juarez-Garia, C.; Munck, E.; Que, L., Jr. *J. Am. Chem. Soc.* **1990**, *112*, 6423–6425.